AD-783 301

AN OPTICAL INSTRUMENT FOR IN-SITU STRESS MEASUREMENT IN ROCKS

TRW Systems Group

Prepared for:

Air Force Office of Scientific Research
Advanced Research Projects Agency

May 1974

AD-783301

DOCUMENT CONTROL DATA - R & D

(Security classification of title, body of abstract and indexing annotation must be entered when the overall report is classified)

1 ORIGINATING ACTIVITY (Corporate author)	2a. REPORT SECURITY CLASSIFICATION
TRW Systems Group	Unclassified
One Space Park	2b. GROUP
Redondo Beach, California 90278	

3 REPORT TITLE

An Optical Instrument for In-Situ Stress Measurement in Rocks

4 DESCRIPTIVE NOTES (Type of report and inclusive dates)

Final Report for period 1 November 1972 - 31 May 1974

5 AUTHOR(S) (First name, middle initial, last name)

Mechanical Engineering Laboratory
Space Vehicles Division

6 REPORT DATE	7a. TOTAL NO. OF PAGES	7b. NO. OF REFS
May 1974	84	13

8a. CONTRACT OR GRANT NO	9a. ORIGINATOR'S REPORT NUMBER(S)
F44620-73-C-0015	
b. PROJECT NO	
ARPA Order No. 2269	AT-SVD-TR-74-6
c. Program Code 3F10	9b. OTHER REPORT NO(S) (Any other numbers that may be assigned this report)
d.	AFOSR - TR - 74 - 1 2 2 6

10 DISTRIBUTION STATEMENT

Approved for public release; distribution unlimited.

11 SUPPLEMENTARY NOTES	12 SPONSORING MILITARY ACTIVITY
	AFOSR/NP
	Arlington, Virginia

13 ABSTRACT

A laboratory model of a holographic instrument, essentially a logging tool, has been designed and tested for measuring in-situ stress in a 9-inch diameter blind exploratory drill hole. The apparatus can ultimately operate remotely at depths of thousands of feet. It has been tested in a simulated borehole in the laboratory on prestressed samples (granite) which upon stress relief produced displacements on the order of .3 μm.

Data, in the form of holographic plates are stored, on board, the instrument. Displacement fields are stored in fringe patterns covering the holographically recorded images of the strained surface. The holographic instrument consists of separate core drill, optics, and laser modules and associated electrical and plumbing connections. The performance of the holographic instrument in a dry and water-flooded simulated borehole was excellent. Good quality holographic interferograms were obtained by double exposure, before and after drilling, in a water-flooded environment, of prestressed slabs of granite under loads in the 130 to 300 bar range.

It is expected that this instrument will be able to resolve principal stresses as low as ~50 bars in dense indurated rocks (moduli ~1 Mbar) and stresses on the order of 5 bars in softer sedimentary rocks having in-situ stresses as low as perhaps ~5 bars (assuming effective moduli of ~100 kbars).

Applications of the instrument include: Geothermal harnessing of energy from hot, dry rock - knowledge of direction and magnitude of principal stress will permit efficient fracturing of rock; estimating excavation costs for deep underground construction; determining stability of opening in deep rocks; discrimination of teleseismic signals to determine their origin (earthquake or explosion); earthquake prediction.

DD FORM 1473 (1 NOV 65)

i

14 KEY WORDS	LINK A		LINK B		LINK C	
	ROLE	WT	ROLE	WT	ROLE	WT
In Situ Stress Measurement in Rocks						
Stress Gage						
Borehole Instrumentation						
Bore Scope or Borehole Camera						
Holographic Instrumentation						

TRW
SYSTEMS GROUP

AN OPTICAL INSTRUMENT FOR
IN-SITU STRESS MEASUREMENT IN ROCKS

FINAL REPORT

1 November 1972 - 31 May 1974

May 1974

AT-SVD-TR-74-6

TRW SYSTEMS GROUP
One Space Park
Redondo Beach, California 90278

if

TRW
SYSTEMS GROUP

FOREWORD

The work reported was performed by several members of the Mechanical
Engineering Laboratory. Contributions are summarized as follows:

Mr. E. K. Burchman	Prestressed specimen preparation Laboratory model fabrication
Dr. D. A. Evensen Dr. A. Kaplan Mr. B. A. Bonnickson	Analytic approach to in-situ stress measurements and computer generation of fringe patterns
Mr. J. L. Jacoby	Optics module
Mr. J. L. Schmidt	Borehole simulation
Mr. G. D. Shaw	Core drill module
Mr. D. R. Tomren Mr. J. E. Martija	Laboratory experiments in simulated borehole
Mr. C. E. Williamson	Mechanical design and layout
Mr. J. E. Wright	Optics module fabrication

In addition to the foregoing, Dr. T. J. Ahrens of the California
Institute of Technology served as a consultant and made valuable contribu-
tions on all aspects of the investigations throughout the course of the
contract including a critical review of the draft of the final report.
Acknowledgment is also made for the interest and review of the project by
Lt. Col. Donald W. Klick and Mr. William J. Best of the Air Force Office
of Scientific Research.

P. G. Bhuta, Manager
Advanced Technology Staff
Mechanical Engineering Laboratory

TRW.
SYSTEMS GROUP

ABSTRACT

A laboratory model of a holographic instrument, essentially a logging tool, has been designed and tested for measuring in-situ stress in a 9-inch diameter blind exploratory drill hole. Conceptually, the apparatus can ultimately operate remotely at depths of thousands of feet in a water-saturated environment. We have to date only tested it in a simulated borehole in the laboratory on prestressed samples (granite) which upon stress relief, in the simulated side walls, produced displacements on the order of .3 µm.

Power and controls for the instrument are at the surface. Data, in the form of holographic plates are stored, on board, the instrument. Displacement fields are stored in fringe patterns covering the holographically recorded images of the strained surface. The holographic instrument consists of separate core drill, optics, and laser modules and associated electrical and plumbing connections. The laboratory model incorporated many features of the field version. The performance of the holographic instrument in a dry and water-flooded simulated (concrete) borehole was excellent. Good quality holographic interferograms were obtained by double exposure, before and after drilling, in a water-flooded environment, of prestressed slabs of granite under loads in the 130 to 300 bar range.

It is expected that this instrument will be able to resolve principal stresses as low as ~50 bars in dense indurated rocks (moduli ~1 Mbar) and stresses on the order of 5 bars in softer sedimentary rocks having in-situ stresses as low as perhaps ~5 bars (assuming effective moduli of ~100 kbars).

Applications of the instrument include:

o Geothermal harnessing of energy from hot, dry rock. Knowledge of direction and magnitude of principal stress will permit efficient fracturing of rock.

o Estimating excavation costs for deep underground construction.

o Determining stability of opening in deep rocks.

o Discrimination of teleseismic signals to determine their origin (earthquake or explosion).

o Earthquake prediction.

TRW
SYSTEMS GROUP

TABLE OF CONTENTS

TRW.
SYSTEMS GROUP

1.0 INTRODUCTION AND SUMMARY

An important geophysical objective is the measurement of the magnitude, and direction, of the in-situ tectonic stresses present within the crust of the earth. Aside from the fundamental value of knowledge of the tectonic stresses present in lithospheric plates, the ability to determine the in-situ stress in deep boreholes is likely to have important applications in the following four areas:

o Geothermal harnessing of energy from hot, dry rock.

o Estimating excavation costs for deep underground construction.

o Determining stability of opening in deep rocks.

o Discrimination of teleseismic signals to determine their origin (earthquake or explosion).

o Earthquake prediction.

In modern concepts of harnessing geothermal energy, one proposes to extract thermal energy in hot, dry rock at considerable depth in the earth. In this scheme one derives heat from hot, dry rock at considerable depth by circulating water in such rock. To increase heat transfer one is required to fracture the rock at sufficient depths to provide increased surface area for improved heat transfer between the circulated water and the rock. For efficient and economical fracturing of the rock at depths of interest, a precise knowledge of the magnitude and direction of the principal stresses is required. The optical instrument described in this report offers the potential to serve as a logging tool for in-situ stress measurement as a function of depth in a pilot borehole. In-situ stress data obtained from the pilot borehole will permit one to more accurately predict fracturing and other associated costs with the development of a particular geothermal site.

For example, knowledge of the basic data related to rock properties is required for the design of openings in rock. Among the required data, information pertaining to in-situ stress field is necessary. Such information is required to both determine the stability of openings and assure safety underground. As mining proceeds to greater depth, in-situ stress field measurements at operational depths become important to production planning. The reduction in risks of rock bursts and cave-ins in a mine is, in general, dependent on the stability of the surrounding stress field

1

(tectonic and overburden) and its long-term response to access tunnels and shafts. Thus, one primary requirement, in addition to knowledge of the underground geology, in the safe design of the mine openings, is the determination of both the magnitude and direction of the in-situ stress fields[1].

Previously available in-situ stress measurement techniques[2,3,4] do not provide a complete measure of the state of stress in the vicinity of the borehole. For example, the Bureau of Mines borehole deformation gage[2], which is currently the best available technique, provides sufficient information to calculate the state of stress in a plane normal to the borehole. In order to obtain a measure of all the components of stress, borehole deformation measurements would be required from three non-parallel boreholes. In calculating the stability of openings, it is also necessary to have a measure of the in-situ stress (tectonic plus overburden) parallel to the axis of the vertical borehole. Disadvantages of the Bureau of Mines borehole deformation gage are that the state of stress at a point is difficult to measure even using three holes and additional expenses are incurred in drilling three holes rather than one. Even after three holes are drilled, the technique provides a measure of three-dimensional average ground stress components because of the nature of the instrumentation used. If this technique were utilized to obtain a measure of the in-situ stresses as a function of depth, the expense incurred would be large, especially if the application is for the design of a deep mine. It should be pointed out however, that the USBM gage is a working instrument.

Ideally, it would be desirable to obtain information pertaining to the three-dimensional stress components as a function of depth from a single borehole. To satisfy this need, TRW Systems has conceived an optical instrument which offers the ability to perform the foregoing. The optical instrument would apply holographic interferometry to the problem of determining stresses in deep boreholes. The advantage of holographic interferometry is that strains can be determined over a large area (several square inches without special surface preparation). Data acquisition rates are limited only by film exposure time and the side hole stress relief drilling operations. The optical instrument, as it would be deployed in the field, is shown in Figure 1.1. As a first step to demonstrate this potential capability, TRW Systems has designed and built a laboratory model of the holographic instrument, capable of operating in a water-flooded simulated borehole environment.

DEPLOYMENT OF
HOLOGRAPHIC BOREHOLE
STRAIN MEASUREMENT PACKAGE
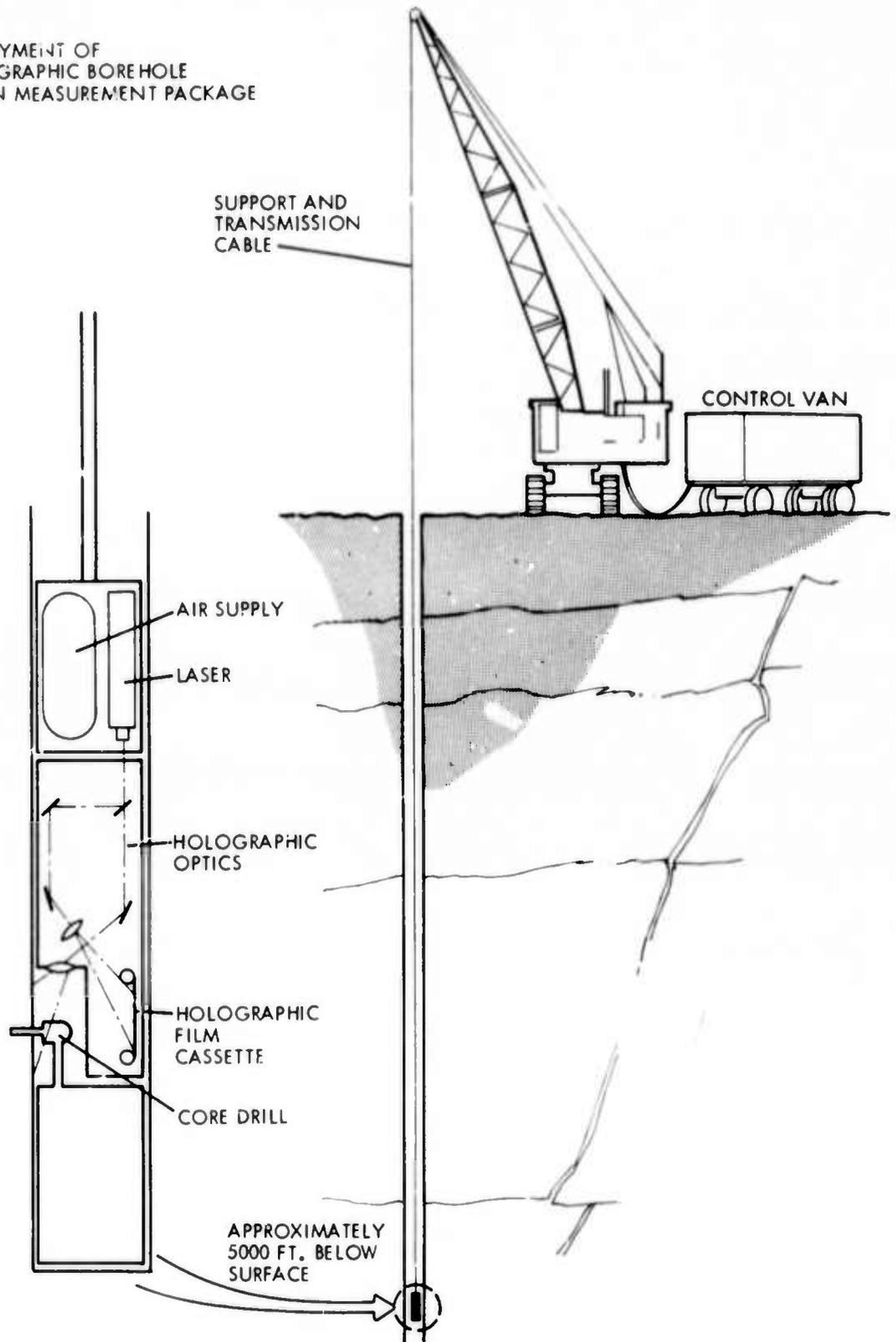
SUPPORT AND
TRANSMISSION
CABLE

CONTROL VAN

AIR SUPPLY

LASER

HOLOGRAPHIC
OPTICS

HOLOGRAPHIC
FILM
CASSETTE

CORE DRILL

APPROXIMATELY
5000 FT. BELOW
SURFACE

Figure 1.1: Optical instrument for in-situ stress measurements.

3

Laboratory experiments conducted with this instrument have established the engineering feasibility of utilizing holographic techniques to measure in-situ stress fields in boreholes.

The principle of operation of TRW's holographic instrument involves measuring the strain relief in the side wall of the borehole caused by drilling a small corehole. The strains are recorded using holographic interferometry where the displacement fields are stored in fringe patterns covering the surface of the specimen. The fringe patterns obtained from holograms conform with those predicted by analytical predictions obtained from the classical theory of elasticity. The fringe patterns are amenable to reduction with the aid of a computer code.

The holographic instrument was designed to operate in a water-flooded nine-inch diameter borehole. The instrument consists of three specially designed modules: (1) core drill module, (2) optics module, and (3) laser module. The core drill module provides the mechanisms for drilling a side corehole in the wall of the borehole while each phase in the underwater drilling operation is sequentially operated from an external control console. The optics module packaged within a waterproof capsule contains the necessary optical components for making a hologram. The laser module provides the coherent light source (laser) for the optics module and is designed to maintain a high degree of optical alignment.

For the present laboratory feasibility demonstration, a simulated 9" diameter borehole was constructed out of concrete. Prestressed rock specimens were attached to a fixture in the wall of the concrete hole so that holographic interferograms could be obtained of the strain relief due to a side core. The core drill module and optics module were held in place within the concrete borehole using a pneumatically driven clamp.

Upon clamping of the optics and drilling modules, the laser is turned on and a holographic exposure is made on the photographic plate. A small 3/8" diameter, ~ 3/8" deep hole is then drilled in the prestressed rock sample. After the drill is withdrawn, the water is allowed to settle and a second holographic exposure is made. The second exposure provides the stress relief data. After processing, the holographic interferogram is reconstructed and the fringe pattern analyzed for a determination of the strain relief around the corehole. In the present experiments, rather than

carrying out a direct inversion, the photo-recorded fringes were directly compared to their computer generated counterparts. The computer generated fringe patterns were calculated from the elasticity solution of the stress pattern around a finite hole in a plate subject to one-dimensional plane stress and the geometry of laser illumination and viewing hologram recon-struction. Initial tests in a simulated borehole have indicated good agree-ment with experiment and theory.

In the field version the measurement of displacement fields as a result of side coring will be carried out at three azimuthal directions around the borehole at a given elevation. The displacement data obtained will provide sufficient information to deduce the three-dimensional stress field present at that point around the borehole. These displacement fields will be utilized to obtain the in-situ principal stresses. Thus, a major future task required for inverting field data to in-situ stress will be the develop-ment of necessary analysis and software for further reducing holographic data. A good start towards this objective has already been made by TRW in this direction for a different application to obtain displacement fields, in a similar geometry, from holographic interferograms. This aspect of in-situ stress data reduction is given in Section 5.0.

TRW

2.0 HOLOGRAPHIC INTERFEROMETRY

The basic concept underlying the measurement of in-situ stress in the optical instrument is to use holographic interferometry to measure all three components of displacement as a function of position produced by the relief of stress around a small corehole which is drilled in the side wall of an existing uncased borehole.

Holographic interferometry is derived from the ability of the hologram to reconstruct a true three-dimensional image of a solid object. The process records both the amplitude and the phase distributions of an optical wavefront (from a laser source) which has interacted with a scene. The hologram is recorded on a standard high resolution photographic emulsion. The image retrieval process, termed reconstruction, reproduces the wavefronts of the light as they existed during the original exposure. An observer, or observing camera, viewing through the hologram sees a virtual image of the scene just as it existed when the hologram was recorded after film development and upon illumination by a laser.

2.1 Double-Exposure Holographic Interferometry

The technique of "double-exposure holographic interferometry" allows one to make precise displacement measurements over the diffuse surface of rocks (Ref. 5). The essentials of the technique used on this program are as follows: First, a single-exposure hologram of the prestressed rock specimen in an underwater environment is made. Then, the rigidly held rock is partially strain relieved by drilling a corehole in the field of view of the instrument. The water is allowed to settle a few minutes and then a second exposure is made on the same holographic plate to form the interferogram. When this "double-exposed hologram" is developed and then reconstructed via illumination with a laser and photographed it is possible to recover the surface displacement of the borehole.

For the present program the interpretation of the fringe patterns obtained from the holograms is accomplished using the technique described by Aleksandrov and Bronch-Bruevich (Ref. 6). It can be shown that the

6

TRW
SYSTEMS GROUP

dark fringes covering the surface of the borehole are located wherever
the condition

$$\vec{\delta} \cdot (\vec{s} + \vec{c}) = \frac{(2n \pm 1)}{2} \lambda \qquad (2.1)$$

is satisfied; where

$\vec{\delta}$ = displacement vector representing the deformation of the borehole wall at a point on its surface

λ = wavelength of the light from the laser used to make and reconstruct the holographic images

$\vec{c}$ = unit vector in the direction from the object to the illuminating source

$\vec{s}$ = unit vector in the direction from a given point on the borehole through the hologram, to the observer

n = integer, ± 1, ± 2, ± 3, ...

The term $\vec{\delta} \cdot (\vec{s} + \vec{c})$ is best understood using the vector diagram depicted in Figure 2.1. The term $(\vec{s} + \vec{c})$ represents a vector bisecting the angle between vectors $\vec{c}$ and $\vec{s}$ having a length $2 \cos 1/2 (\vec{s}, \vec{c})$. Hence the term $\vec{\delta} \cdot (\vec{s} + \vec{c})$ represents the component of deflection, $\delta_{c,s}$ in the direction of a unit vector bisecting the angle between the viewing and illuminating direction times a factor $2 \cos 1/2 (\vec{s}, \vec{c})$. Hence, Equation (2.1) can be written

$$\delta_{c,s} = \frac{(2n - 1)\lambda}{4 \cos 1/2 (\vec{s}, \vec{c})} \qquad (2.2)$$

Qualitatively, the fringes seen over the object represent lines of constant displacement in the direction of the vector $\vec{c} + \vec{s}$. If parallel light is used to illuminate the object and the angle subtended by the object from the position of the observer is less than 1°, then the vector $\vec{c} + \vec{s}$ can be considered constant for all points on the object surface.

The total displacement field of the borehole wall is obtained by appropriately varying the illumination and viewing direction and hence,
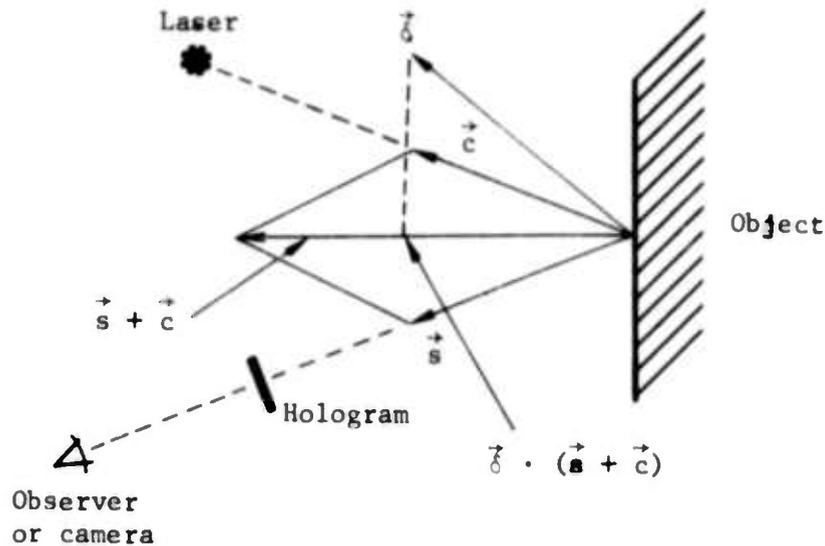
7

Figure 2.1: Vector diagram showing the relationships between the vectors used in Eq. (2.1).

the direction of the vector, $\vec{c} + \vec{s}$. Once the total displacement field of the borehole wall induced by stress relieving a small volume of rock around the side core is obtained, the stresses existing <u>before</u> both the main borehole and "side" corehole were drilled must be inferred using the theory of elasticity and knowledge of the elastic properties of the rock formation being tested. The appropriate stress analysis for the case of our laboratory tests in rock samples under conditions of pre-existing simple plane compression and the general case of determining the principal stress tensor with arbitrary orientation with respect to the borehole, is given in Sections 5.0 and 6.0. A discussion of the analysis of stress relief in plane cylindrical geometry is given in Appendix A.

One of the major accomplishments of the project, in the use of holographic interferometry in a borehole, was the achievement of the relative stability of the optical components between hologram film exposures, i.e., during the time the side corehole is being drilled. Although some movement of the optical components relative to the borehole is tolerable, movements of the optical components more than ~ 0.006 mm, or ~ 10 optical wavelengths is not acceptable. Rigid body displacement

8

of the optics, between exposures, can give rise to a series of
approximate parallel fringes on the resulting holograms. As long as
rigid body displacements do not exceed several light wavelengths,
the nominal number of "finite fringes" superimposed on the strain
induced fringes can be removed in numerical analysis of the resulting
holograms.

2.2 Finite Fringe Double-Exposure Holographic Interferometry

The technique of finite fringe interferometry is a slight variation
of conventional double-exposure holographic interferometry (Ref. 7).
The essentials of this technique are identical to those described in
Section 2.1 except that a controllable induced displacement takes place
between exposures. This creates a uniform pattern of fringes which are
a function of the amount and direction of the displacement. Nearly
straight fringes can be created when the displacement is along a single
axis. The operator induced fringe pattern interferes with the strain
relieved fringe pattern to yield a composite fringe pattern. Relief
will be measurable out to the beginning of the fringe departure from
the background fringe pattern.

The induced fringe density, as well as fringe orientation, are
important for this technique to work in a real borehole atmosphere.
In the laboratory version the rock specimen support was displaced
between exposures. In the field, the holographic film plane could be
equivalently displaced to yield identical results.

TRW
SYSTEMS GROUP

3.0   LABORATORY MODEL DESIGN APPROACH

A study was performed on a hypothetical operational field unit to define the system requirements. Based on this system definition, design requirements were formulated for the laboratory model.

Pre-design experiments were performed to solve engineering problems and to insure a sound and workable design. A three-dimensional composite design concept was made to determine how to best package all the components into the limited space within the design requirements. This approach provided a realistic feel for the design without using a fabricated model.

Two sets of experiments were performed before detailed design sketches were prepared. The first involved investigation of various optical arrangements for the holographic optics module. This was to insure that the most efficient arrangement from a space standpoint was used and to insure that the design would provide holograms of consistent quality during extended operations. The second set of experiments involved finding the mechanical requirements for the core drill module so that the smallest possible package could be designed.

The following guidelines for the laboratory version were established based on the system study and laboratory convenience:

1. Only the holographic optics module, the core drill module and the hole locking mechanisms were packaged for testing in a water flooded environment. The laser module was sized to fit in a 9-inch hole but was primarily designed only to support the laboratory experiments without operation in a water flooded environment.

2. All other support functions were kept external to the laboratory simulated borehole (i.e., the laser, all electric power supplies, fresh water supply, etc.).

3. The holographic optics recording module was mechanically isolated during the corehole drilling operation.

4. The holograms were recorded on 4" x 5" glass holographic plates while a mechanized film cassette would be needed in the field version for data storage.

10

5. The core drill module was designed so that the core drill could be removed from the field of view during film exposures. At the same time, the module was designed such that a sufficient variable drill feed force could be provided for the drilling operation.

6. The optical arrangement for obtaining the holographic interferograms was such that a single laser beam would provide sufficient rock surface illumination.

7. The core drill module was internally pressurized to prevent water from leaking through various seals while the optics and laser modules were unpressurized. In the field operation, positive air pressure equal to the ambient pressure will be maintained on the interior of the modules to offset that of the outside water.

8. The simulated borehole was constructed of concrete with a nine-inch hole. Two ports were built-in to the concrete to aid in the collection of holographic data. The specimen port was designed for easy insertion of prestressed flat specimens while the viewing port was designed for checking optical alignment and simplified removal of holographic plates.

The final laboratory version is sketched in Figure 3.1. A description of the final prototype modules and simulated borehole is given in Sections 3.1 to 3.4.

3.1 The Core Drill Module

The core drill module provides the mechanisms for drilling the side core hole in the prestressed rock specimen between holographic exposures. The main features of the module, shown in Figure 3.2, are: The lower housing which contains the drive and feed motors as well as other auxiliary pneumatic and electronic components; and the extendable drill head which houses the right angle drive and the drill core bit. The drill head can be raised and lowered so that it will not be within the field of view during the holographic exposure. A pneumatic cylinder is used to control this operation. The drill bit is operated by means of a specially designed 2-7/8 inch diameter motor which is powered by 24 volts D.C. and ~3 amperes and provides 30 in-oz of torque at 4000 RPM. This motor is located in the lower housing

11

TRW
SYSTEMS GROUP

LABORATORY TESTING OF
HOLOGRAPHIC BOREHOLE
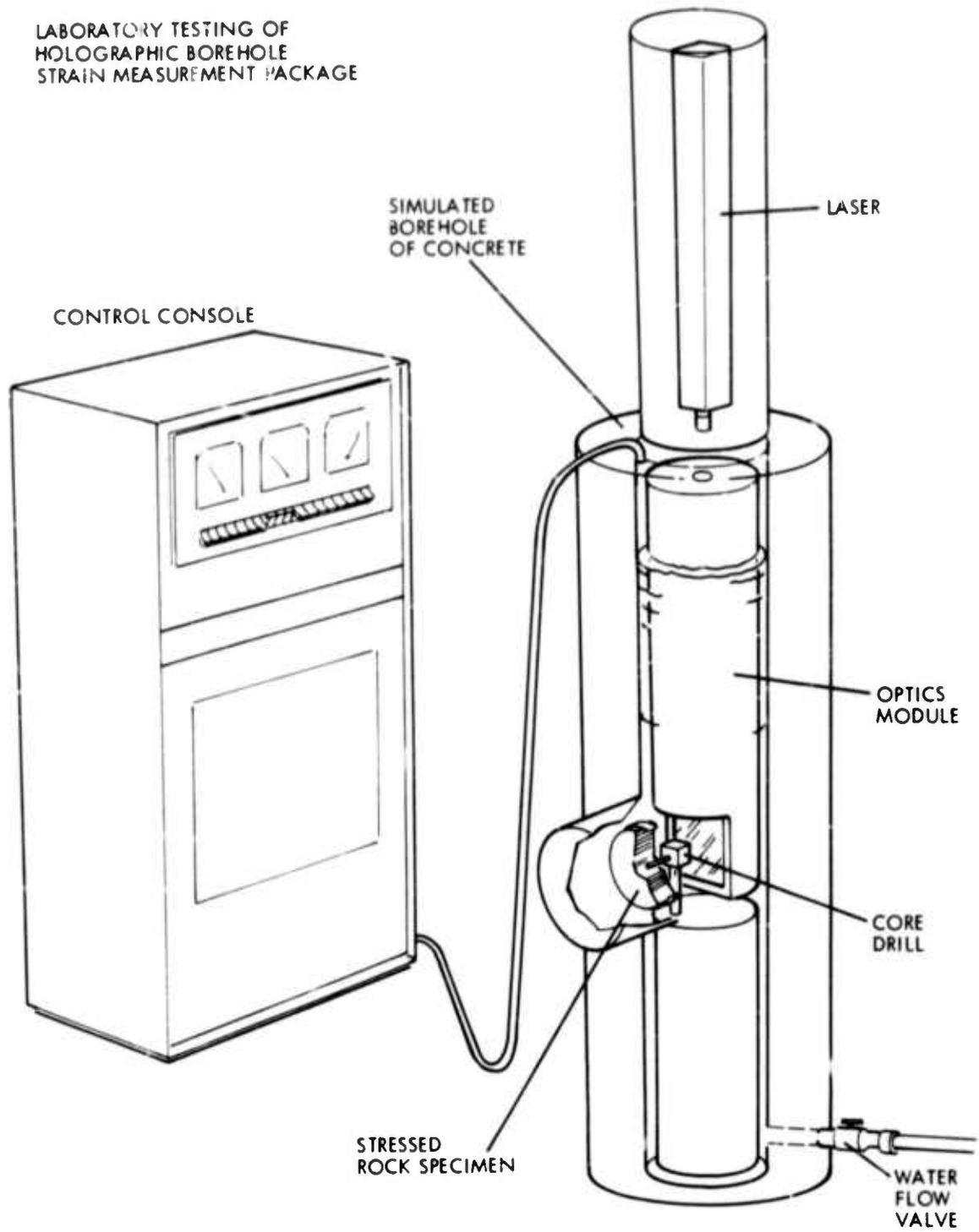STRAIN MEASUREMENT PACKAGE

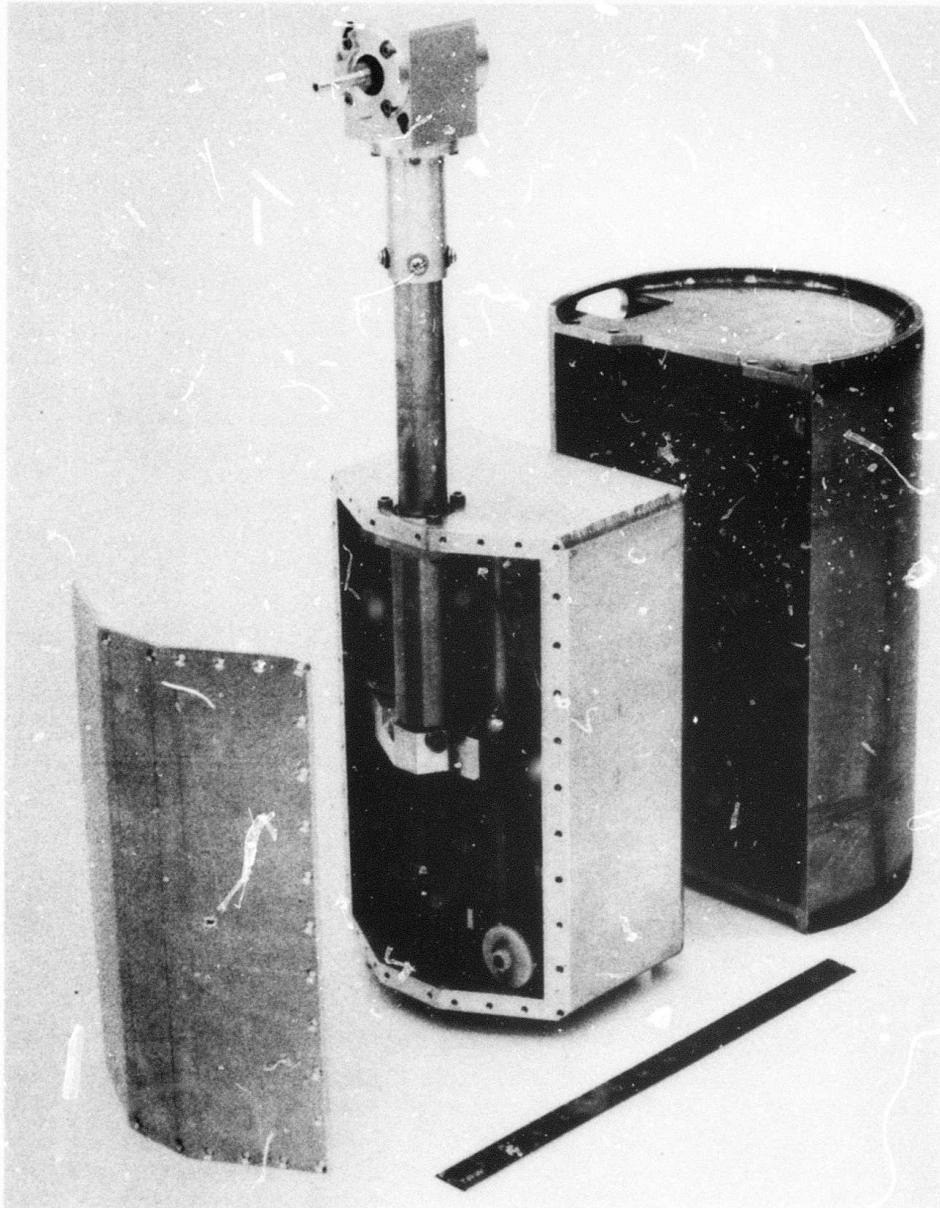Figure 3.1:   Laboratory simulation of borehole instrument.

12

Figure 3.2: Photograph of the core drill module components. The right angle core drill head is pneumatically raised and lowered out of the core drill drive assembly. In turn, the core drill drive assembly is moved in and out of the support housing via a lead screw mechanism to provide the drilling motion.

13

and is connected to the drill by means of a linkage within the drill head extension arm. The right angle drive in the drill head was specially designed to transfer a high torque to the drill bit and yet fit into the small space dictated by the geometry of the borehole configuration. Once into position, the core drill is advanced into the rock specimen by means of a small lead screw motor contained in the lower housing. This is a low speed, high torque motor which is also operated with 24 volts D.C. The lead screw mechanism operates by moving the complete core drill inner housing assembly in and out of the outer module steel housing on two support pins. The maximum side core drilling capability in the present configuration is approximately one inch. The steel core drill module outer housing is held stationary in the borehole, independent of the optics module, by its own pneumatically driven locking mechanism.

The diamond core bit (1/4 inch or 3/8 inch diameter in the present experiments) is connected to a hollow shaft which extends out the rear of the drill head. A small suction tube is attached to this shaft for the removal of debris during the coring operation. This concept is exactly opposite to that normally used to remove cuttings from core drills. It prevents the debris from clouding the water around the specimen and obstructing the field of view. In a field deployment operation, this technique will also be used to filter muddy or clouded water in the vicinity of the holographic viewing area.

3.2 The Optics Module

The optics module consists of a cylindrical package which contains all of the optical components required for making a hologram of the side wall of the borehole. The module consists of an internal optics support structure packaged within a cylindrical waterproof anodized aluminum capsule. The internal "skeletal" structure, shown in Figure 3.3, consists of four steel threaded rods to which the optical support fixtures are attached. These rods were ground to tight tolerances to allow the fixtures to slide with minimum play and yet not bind up on the threads. Hexagonal nuts are used to rigidly hold each support fixture in position. This approach allows gross adjustment of the optical elements to be made on the support rods while final adjustments are made with the use of set screws behind the key
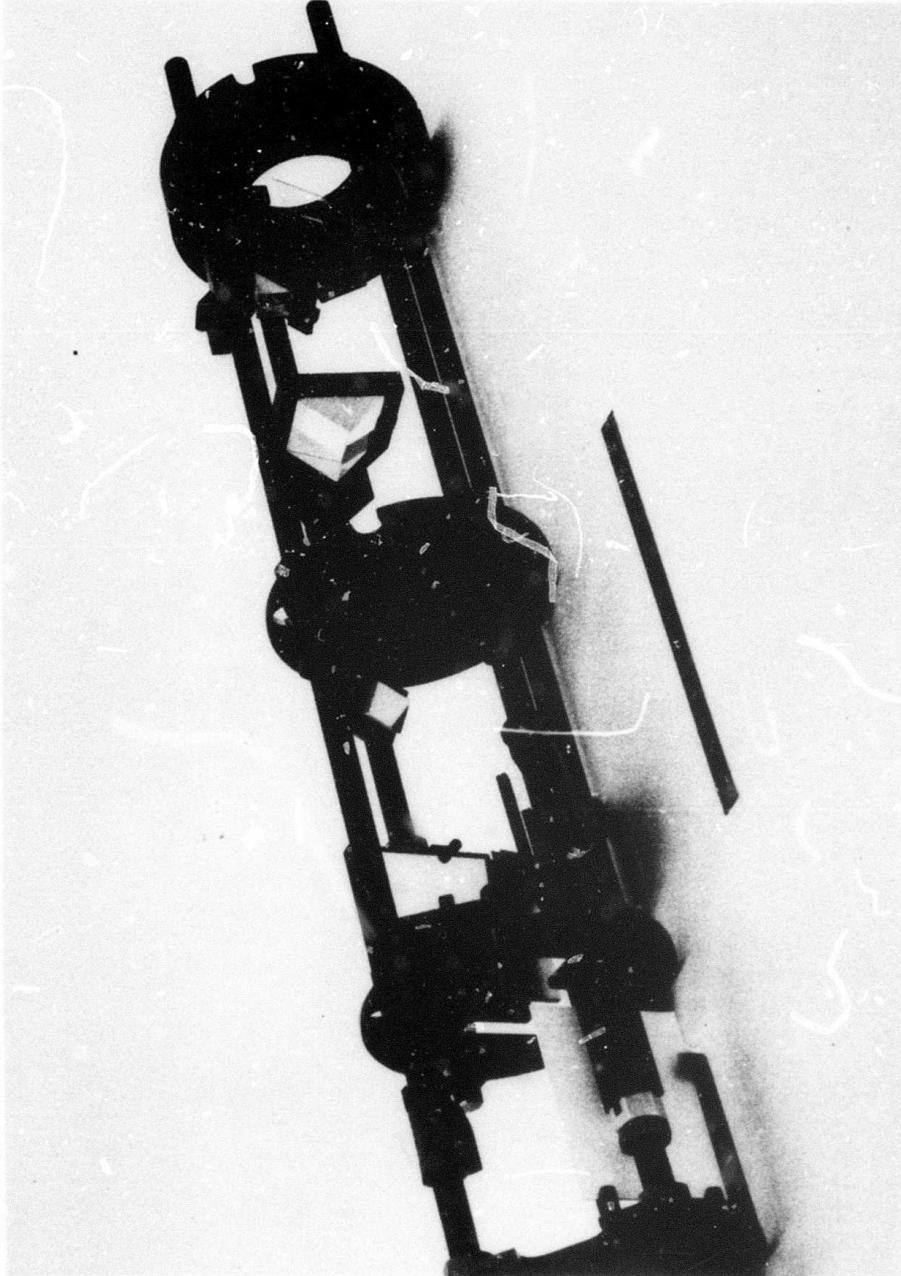
14

Figure 3.3: Photograph of the holographic optics support structure. The threaded rods and bulkheads provide rigidity for the optics while providing versatility in the adjustment of the elements.
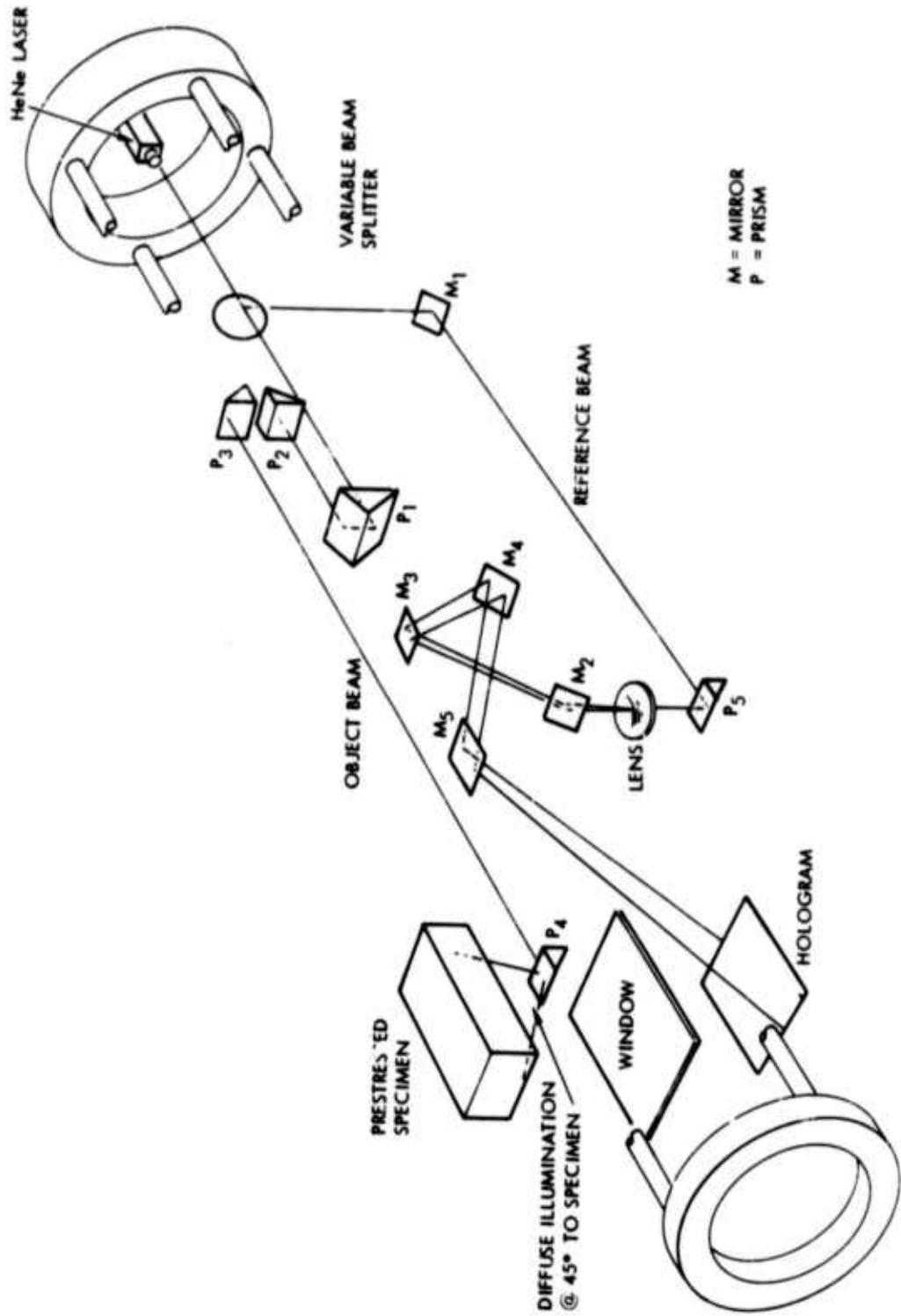
Figure 3.4: Schematic view of optics module layout.

optical elements. The structure is made rigid by bracing the rods between three aluminum bulkheads. The holographic film plate location is further strengthened by two additional bulkheads. This very rigid structure is needed in order to prevent any optical path length changes during or between the holographic exposures in the borehole environment.

A breakaway view of the internal optics structure is shown schemati-cally in Figure 3.4. Referring to this figure, the light from the laser module enters from the right and is split by a variable beam splitter into two beams, the object and reference beams. The prisms in the object beam can be adjusted so that its path length can be accurately matched to that of the reference beam as required by the holographic process. The final prism in the path of the scene beam has a rough surface which serves to uniformly diffuse the light onto the specimen. The diffuse reflection from the rock specimen reflects back through the window and onto the 4" x 5" holographic plate where it interacts with the reference beam. The refer-ence beam was expanded by a negative lens and routed with adjustable mirrors until it covered by 4" x 5" film plate.

The module contains three glass windows. A small round (40 mm diameter) window located on the top of the module is the entrance point for the laser beam (from the laser module). A second 40 mm diameter window, located in the plane of the specimen and the hologram, allows the scene beam to exit the module and illuminate the specimen. The third window is a relatively large (115 mm x 190 mm) rectangular viewing port located directly between the hologram and the specimen. A removable aluminum cover plate is located in the outer capsule immediately behind the hologram. This allows easy access to the hologram before and after the tests. It is also possible to adjust the reference beam lens with this plate removed. In the same manner as was used with the core drill module, the optics module was held rigidly in the hole by means of a pneumatically driven locking mechanism.

The complete optics module (without its waterproof capsule) is shown in Figure 3.5 along with the core drill module described in the previous section.
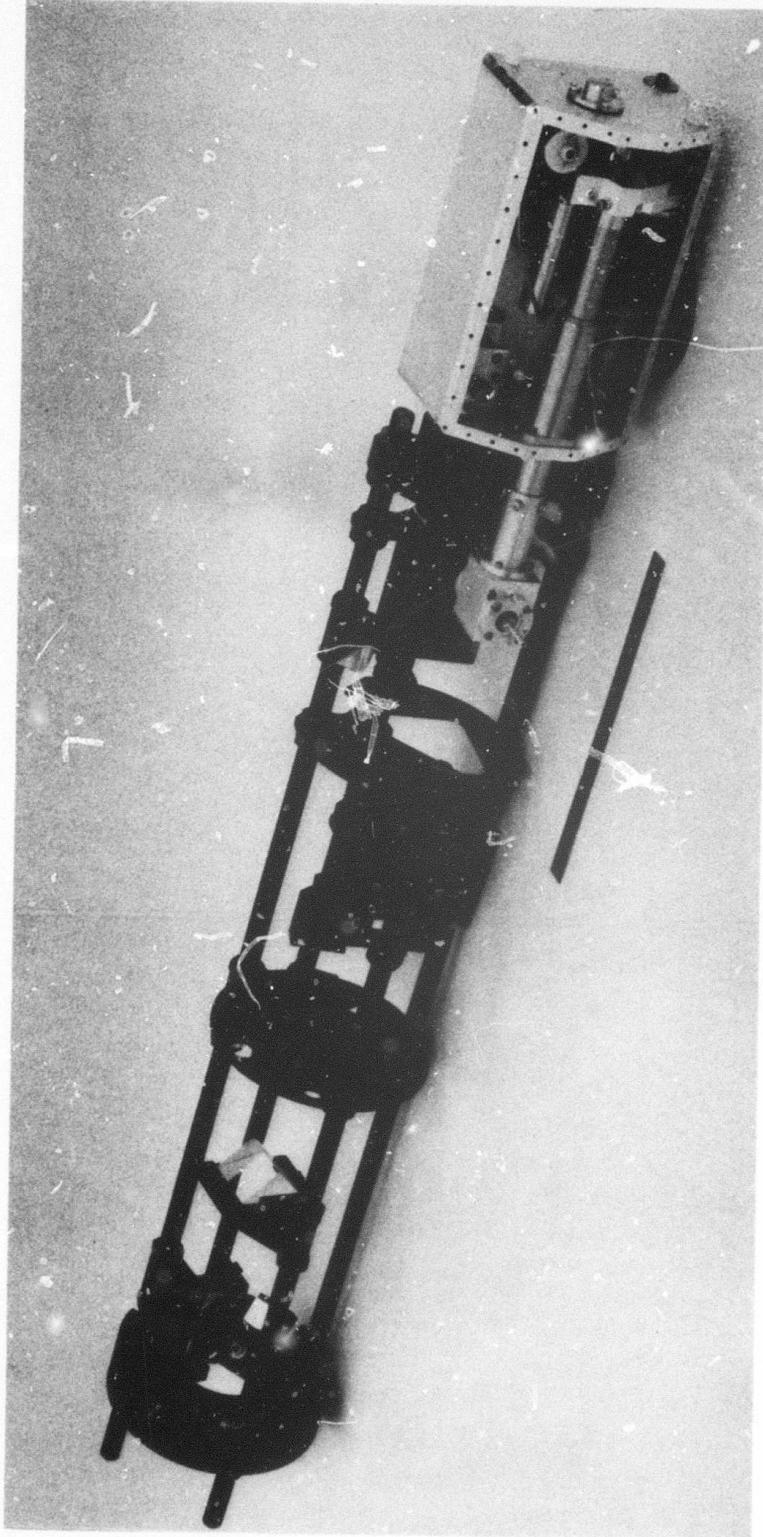
17

Figure 3.5: Photograph of internal parts of the optics module and core drill module in approximate orientation for drilling.

TRW
SYSTEMS GROUP

3.3 Laser Module

The laser module was designed for laboratory using an existing TRW laser. The laser module consists of a standard Spectra Physics 15 mw HeNe laser mounted vertically in a nine-inch diameter cylindrical capsule. The laser is rigidly attached to the inside of the capsule with the optical axis of the laser beam near the center of the capsule. A laser beam steerer, consisting of two adjustable mirrors, is used to align the beam into the beam splitter located in the optics module. The laser module is mated to the optics module by locking hexagonal nuts to the four threaded rods protruding from the optics module. No effort was made to capsulate the laser in a waterproof housing since it would not be subjected to water-flooded environment during the laboratory tests. In the field version the laser and power supply would be packaged to withstand the anticipated deep borehole environmental conditions.

3.4 Simulated Borehole Preparation

A simulated laboratory borehole was required to demonstrate the capabilities of the laboratory model. Ideally, a simulated borehole would have consisted of a cylindrical nine-inch diameter wall of water-saturated stressed rock taken from a deep borehole environment. Since this was not possible, the following compromises were made to best simulate a deep borehole environment within the confines of the laboratory: (1) the laboratory borehole was constructed of concrete capable of being filled with water, (2) high stress concentrations in rocks were simulated with flat prestressed granite specimens, and (3) holographic plate removal was simplified with an access port in the concrete borehole and cover plate in the optics module since a film cassette was not a part of the laboratory model to demonstrate engineering feasibility of in-situ stress measurement.

The simulated borehole shown in Figure 3.6 was cast in a standard reinforced concrete form (24 inches in diameter and 68 inches high) with a central through hole (9 inches diameter). Two anodized aluminum ports were added prior to casting to aid in collecting holographic information. The round specimen port was 15 inches in diameter and was capable of handling prestressed flat rocks (round or rectangular) up to 5.5 inches in diameter. Specimens were held in position with star-like aluminum fixture and were indexed by a symmetrical four bolt pattern. Water sealing was achieved

19
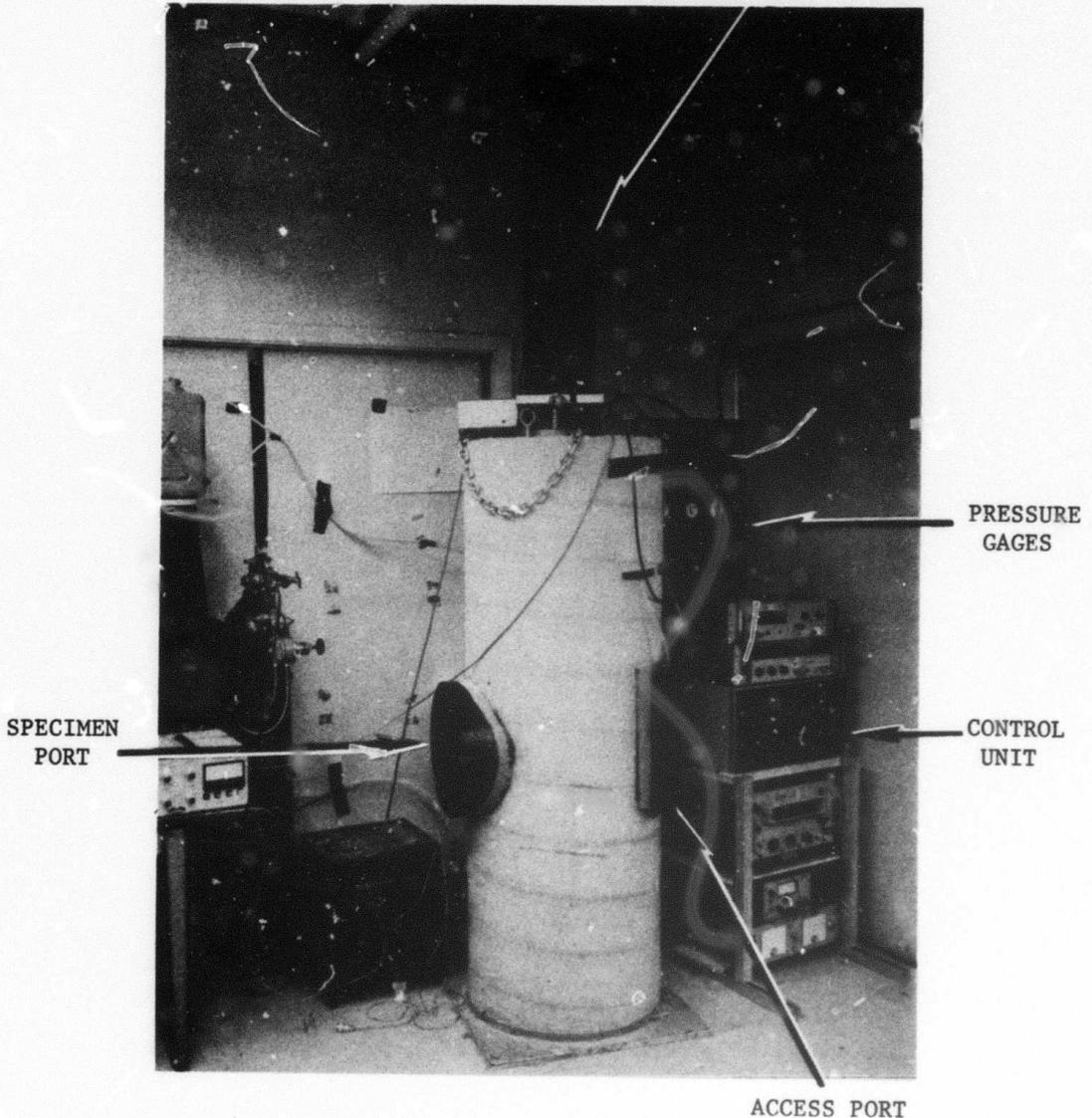
Figure 3.6: Concrete borehole with associated electrical and plumbing connections to the core drill and optics modules (positioned out of view in the concrete borehole). The 24 volt power supplies, pressure gages and control unit is on the right of the concrete borehole. The rectangular access port on the right side of the borehole is for viewing and installing holograms. The cylindrical opening on the left side (partially hidden) is for specimen installation. The black cylinder on top of the borehole is is the laser module. Plastic water reservoirs and laser shutter control are located to the left out of the field of view.

either by a compressed O-ring or by RTV sealant. The rectangular access port (8 inches x 15 inches) simplified the removal of holographic plates during testing by not having to unclamp and remove the optics module after each test. A drain hole was incorporated at the bottom for filling and draining water in the borehole. Water was stored in a plastic reservoir and allowed to fill the borehole by gravity. Water was returned to the same reservoir with a small water pump.

The core drill module was positioned in the borehole for drilling a hole in the center of the specimen opening. The core drill module was pneumatically held in place to the concrete wall with a clamping cylinder and support pads. The associated plumbing and electrical connections to the control box were interfaced to the core drill module. The control box was designed with interlocks for sequencing the drill operation (i.e., raising, advancing, drilling, retracting, lowering). A tabulation of the installation and checkout procedure is given in Figures 3.7 and 3.8.

The optics module with its coated optics was aligned prior to insertion into its environmental capsule. The optics module was then mated to the laser mdoule and bench tests were conducted to insure alignment stability and optimum exposure settings. The two modules were disconnected and each installed individually into the concrete borehole. The optics module was pneumatically held to the concrete wall in a manner similar to the core drill module. The laser module, consisting of a 15 mw HeNe laser and beam steerer, was locked with hexagonal nuts to the four threaded rods of the optics module described in Section 3.2. Additionally, a ring was attached to the laser module to prevent the lower optics module from slipping in the event of loss of air pressure.

3.5 Prestressed Rock Techniques

Two fundamentally different techniques were used to prestress granite rock for the borehole simulation tests. A simple approach (shown in Figure 3.9 and analyzed in Section 6.0) was selected as the primary method of inducing approximately plane stress, prestresses in rock specimens. Here, a rectangular block of White Sierra granite (2" x 4" x 5.75") obtained from Mojave Granite Co., Los Angeles, California, was uniaxially loaded in compression from two sides with two quarter point positioned steel ball bearings.

TRW
SYSTEMS GROUP

Figure 3.7: Summary table of holographic instrument
installation and checkout procedure in
simulated borehole.

STEP	DESCRIPTION OF INSTALLATION	CHECKOUT
1	Lower, align and lock core drill module into position for drilling perpendicular to the specimen opening.	Monitor sidewall locking with pressure regulator C-1 and gage G-1 (~150 psi) on control panel (N_2 bottle).
2	Pneumatically raise and lower drill head of core drill module.	Monitor with pressure regulator R-2 and gage G-2 (~50 psi) on control panel (house air pressure).
3	Lower and lock optics module into position for unobstructed viewing of the specimen opening. Align optics module window perpendicular to the drill head of the core drill module.	Monitor sidewall locking with pressure regulator O-1 and gage G-1 (~150 psi) on control panel (N_2 bottle).
4	Lower and lock laser module to optics module with four hexagonal nuts to the four protruding threaded rods of the optics module.	Verify object and reference beam alignment with laser.

Figure 3.8: Summary table of control box checkout and drilling procedure.

STEP	DESCRIPTION OF CONTROL BOX	FUNCTION	CHECKOUT
1	Verify switch positions on console after hook-up to two 24 volt power supplies:	Power to control box.	Check with voltmeter.
	Shutter Switch (SW-A)	Lights to indicate power to laser shutter or core drill module.	Light L-1 "shutter." Light L-2 "core drill module (CDM)."
	Up/Down of Drill Head (SW-1)	Lights to indicate "up" or "down" position of drill head.	Light L-3 "down." Light L-5 "up and locked."
	Arm Drill Head (SW-2)	"On" position indicates drill head cannot be lowered once drill head is in "up" position.	Light L-5 remains lit even if SW-1 is switched "off"
	Suction Pump (SW-3)	Power to suction pump leading to drill head.	Check with voltmeter.
	Drill Motor (SW-4)	Light "on" to indicate drill motor operation.	Light L-7.
	Advance/Retract (SW-5)	Light "on" to indicate drill head in fully retracted position. Light "off" indicates drill head has advanced.	Light L-4.
2	Move switch SW-A to "CDM" position after main power is "on."	Power supplied to core drill module for drilling operation (SW-A to "shutter" would be for laser exposure).	Lights L-2, L-3, L-4 should be "on" and others "off."
3	Move SW-1 to "up"	Pneumatically lift drill head into drilling position (L-5 comes "on" only at full extension of stroke).	Lights L-2, L-4, L-5 should be "on" and others "off."

Figure 3.8: Summary table of control box checkout and drilling procedure (cont.).

STEP	DESCRIPTION OF CONTROL BOX	FUNCTION	CHECKOUT
4	Move SW-2 to "Arm Drill"	Prevents drill head from being prematurely lowered.	Light L-5 remains "on" even if SW-1 is switched "off."
5	Move SW-3 to "Suction"	Suction pump is operated only in underwater environment to remove debris in water.	Monitor on gage G-4.
6	Move SW-4 to "Drill"	Drill speed operates up to 4000 RPM as a function of input voltage. Speed is measured from magnetic pick-up in core drill module.	Lights L-2, L-4, L-5 L-7 should be "on" and others "off." Verify speed with digital counter.
7	Move SW-5 to "Advance"	Drill head advances toward specimen opening. Feed rate controlled by variable resistance feed pot. Distance measured by variable resistor in core drill module.	Light L-4 must turn "off" while L-2, L-5, L-7 remain "on." Monitor advancement with digital voltmeter.
8	Reverse steps 7, 6, 5, 4, 3, 2	Retract lower drill head in preparation for laser exposure.	Lights for each step (7-2) should be verified.

24

TRW
SYSTEMS GROUP

HEXAGONAL NUTS FOR
ADJUSTING LOAD

STEEL RODS WITH
STRAIN GAGES

QUARTER POINT
POSITIONED BALL
BEARINGS ONTO
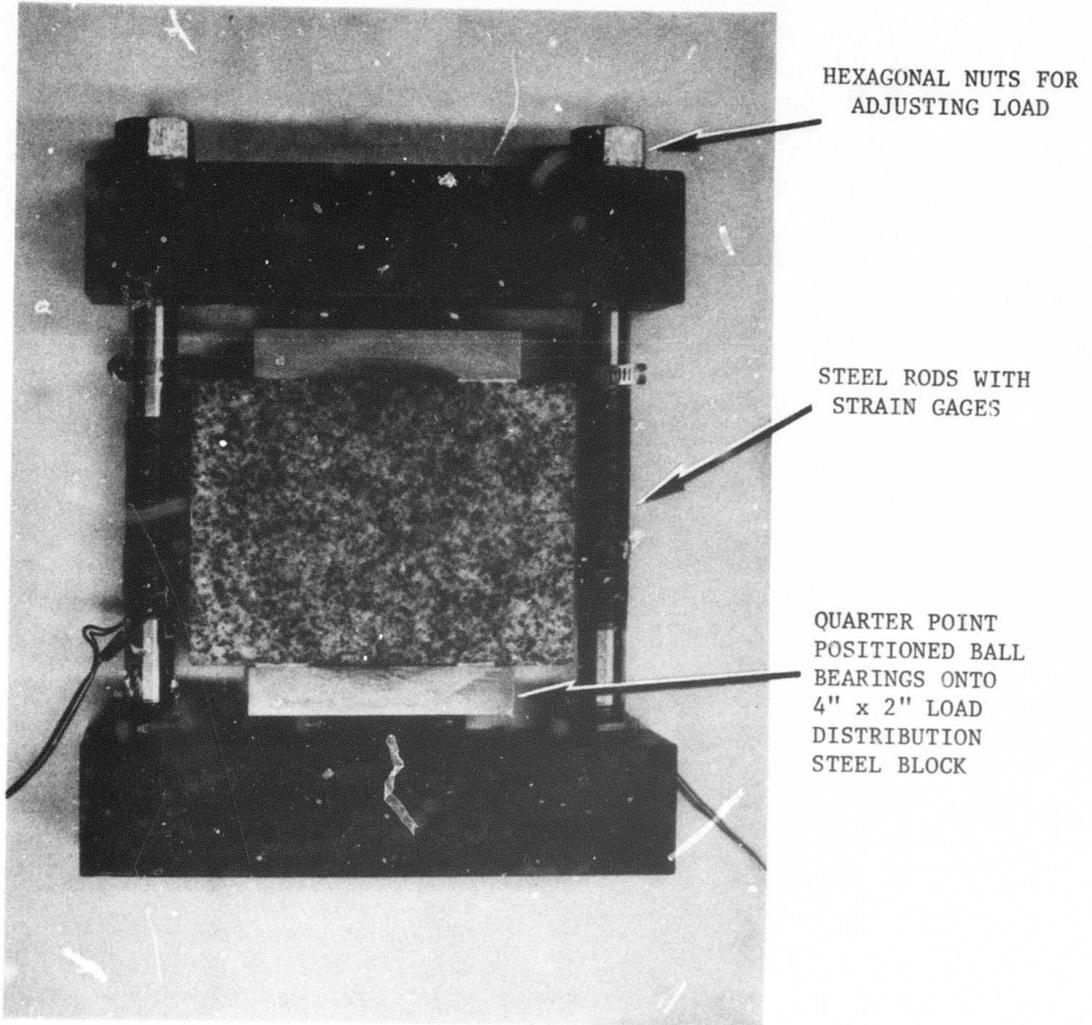4" x 2" LOAD
DISTRIBUTION
STEEL BLOCK

Figure 3.9: Uniaxial loading fixture for flat granite specimens (2" x 4" x 5.75"). The hole in the center is from the 1/4" core drill. The rods are strain gaged for monitoring while loading the specimen. Loading is accomplished by tightening the hexagonal nuts on top.

TRW
SYSTEMS GROUP

Rosette strain gages were applied to the steel rod so that the load could
be monitored. The rods were loaded equally by tightening the two hexagonal
nuts which in turn loaded the rock. The steel rods were calibrated in a
Baldwin loading machine using strain gages. A strain gage was attached to
a granite specimen in the loading fixture and correlated with the actual
load and the rod calibration. Additionally, a strain gage was attached to
each rock specimen to insure the achievement of a known strain level. The
strain gage calibration curve for a White Sierra granite rectangular speci-
men is shown in Figure 3.10.

In the cylindrical specimen we attempted to achieve uniform compressive
two-dimensional strain by shrinking a machined steel ring over a ground
cylindrical granite specimen. The rock specimens were specially ground
cylindrical disks of White Sierra granite 2 inches thick and $\sim$ 6 inches in
diameter by slipping a heated steel ring over the granite disk and letting
it cool to create a two-dimensional compressive stress. This approach was
intended to provide a symmetrical radial distribution of displacement; however,
insufficient prestress levels were obtained from shrink-fit. The rectan-
gular specimen approach was easier to implement and offered several
advantages such as: (1) adjustable stress levels, (2) savings in machine
time (no accurately machined steel rings or round specimens required), and
(3) quick turnaround time in obtaining rectangular specimens.

Disadvantages of this geometry included: (1) only an approximate state
of plane compression is possible with a finite size rock sample, and
(2) compressive stress applied by platens is inherently nonuniform at edges
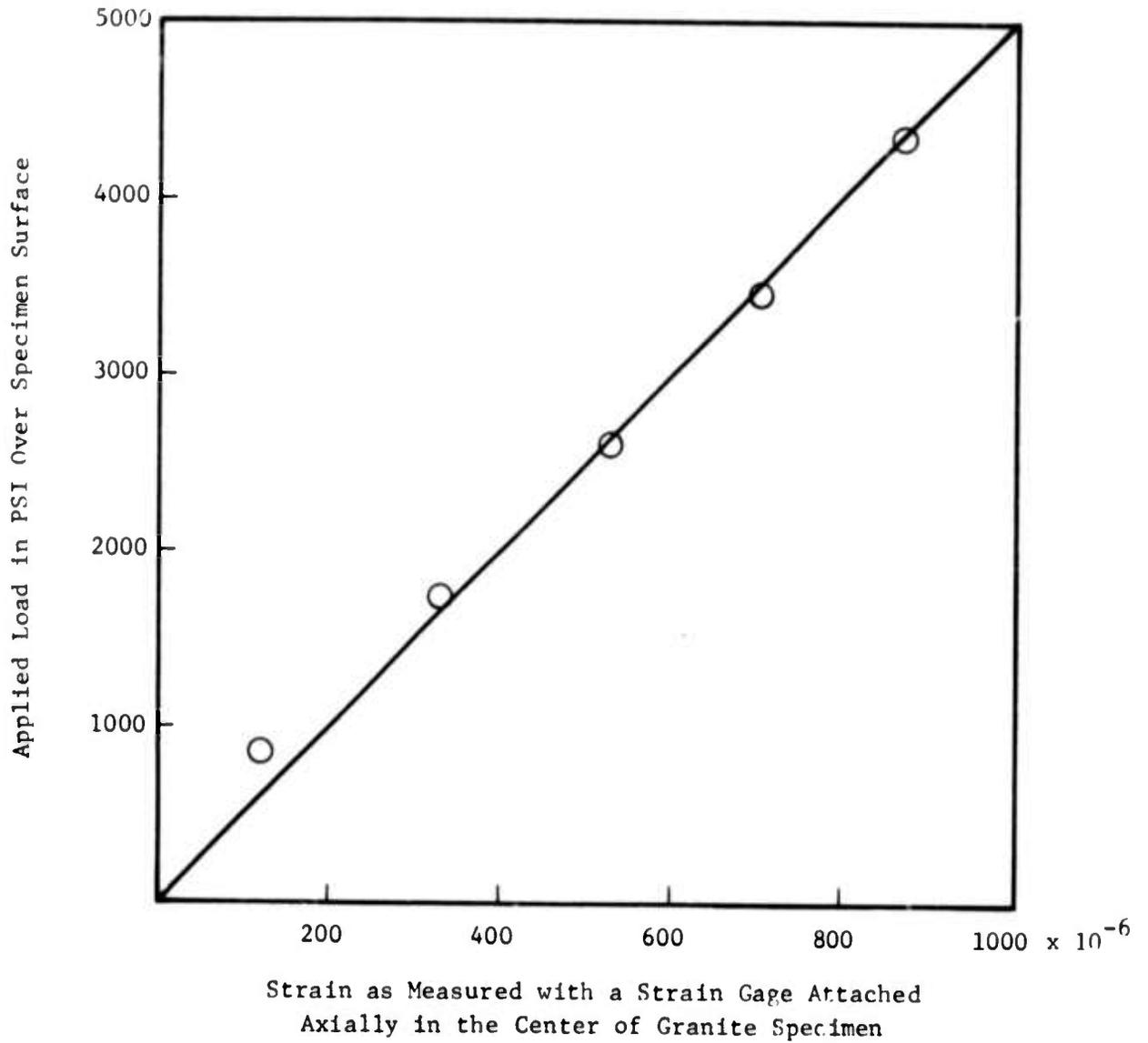of steel bearing plates.

26

Figure 3.10: Calibration curve for loading rectangular
White Sierra granite.

TRW

4.0 LABORATORY EXPERIMENTS IN THE SIMULATED BOREHOLE

Using the concepts described in the previous section, approximately twelve definitive tests of the new borehole holographic technique we have developed were carried out. Initially, a rigorous step by step procedural check out of the instrumentation was performed. Each step in the drilling operation was verified to be functioning as designed. (See Figure 3.7 and 3.8 in Section 3.4.) The film used for the holographic tests was Agfa-Gevaert 10E75 4" x 5" anti-halation glass plates. In a dry environment high brightness fringe-free single exposure holograms were readily obtained with a minimum exposure of one second and normal development of 3-4 minutes in Kodak D-19 developer using our 15 mw laser.

Likewise high brightness fringe-free double exposure holograms were readily obtained in a dry environment with minimum individual exposures of one-half second. Moderate to high brightness fringe-free single exposure holograms were readily obtained in a clean water-flooded environment with minimum exposures of one to two seconds (developing in Kodak D-19 developer). Moderate to high brightness fringe-free double exposure holograms were obtainable with individual exposures of one-half to one second in a clean water-flooded environment. When the spatial variations in water temperature and turbulence had decayed, little or no difficulty was encountered in taking double exposure holograms with up to ten minutes between exposures. For long times between exposures, (i.e., > 5 minutes), there was typically one to three broad fringes due to some form of uninduced displacement without actually drilling a hole in the specimen. These fringes were generally out-of-plane to the granite surface and did not seriously affect the results. When we did not wait for steady conditions in the water to prevail, filamentary fringing could be seen in holograms. This problem was readily overcome by allowing the water to thoroughly settle prior to making both the first and second exposures. In virtually all our holograms some finite fringing was obtained such that some fringes from rigid body displacement were superimposed on the fringe pattern produced by strain relief. The direction of displacement was identical in most cases as evidenced by the same fringe orientation. Thus, the rigid body displacement can probably be attributed to the method of specimen support or the instrumentation clamping

system in the simulated borehole. In the field version, because of the larger mass surrounding the borehole, more stable conditions would be expected to prevail which should minimize extraneous fringes.

As operator confidence in the instrumentation improved during the check-out procedure, the time required for making test holograms was reduced from 30 minutes or so to 10 minutes. In general, at least one finite fringe hologram was made of each specimen in a dry environment to insure good fringe contrast. The fringes were induced by slightly unloosening the star-like fixture holding the specimen between exposures. The borehole was filled with water and allowed to settle for 10 minutes prior to making either double exposure holograms or finite fringe interferograms. In general, at least one finite fringe interferogram and/or double exposure hologram was made with periods between exposures ranging from five to ten minutes. These time delays were representative of the amount of time required to allow for water turbulence to be minimized and for all drilling functions to be checked out. The procedure followed in the drilling process was to make a single exposure hologram with all functions off in an underwater environment as shown in Figure 4.1. The rock was sequentially drilled to approximately one core drill diameter and retracted to the down position. The second exposure on the same plate was made three minutes after all drilling functions had ceased. During this time, the rock support was either left undisturbed for a double exposure hologram or slightly unloosened to obtain a finite fringe interferogram.

4.1 Holographic Results of Strain Relief Fringe Patterns

The entire test series conducted on this program to verify the feasibility of obtaining strain relief fringe patterns of a prestressed rock in a simulated borehole is summarized in Figure 4.2. Initial tests were all conducted with a 1/4" drill at various prestress specimen levels with the first indication of lobe patterns noted close to the drilled hole. Operator controlled finite fringe double exposure holograms with varying fringe densities (4-6 fringes/inch seemed the most effective) also demonstrated strain relief around the drill hole. Since the fringe patterns created with the 1/4" core drill extended only a small distance from the hole (i.e., < 1/2"), a larger 3/8" drill was employed. The tests with the 3/8" drill exhibited greater fringe displacements and hence greater strain
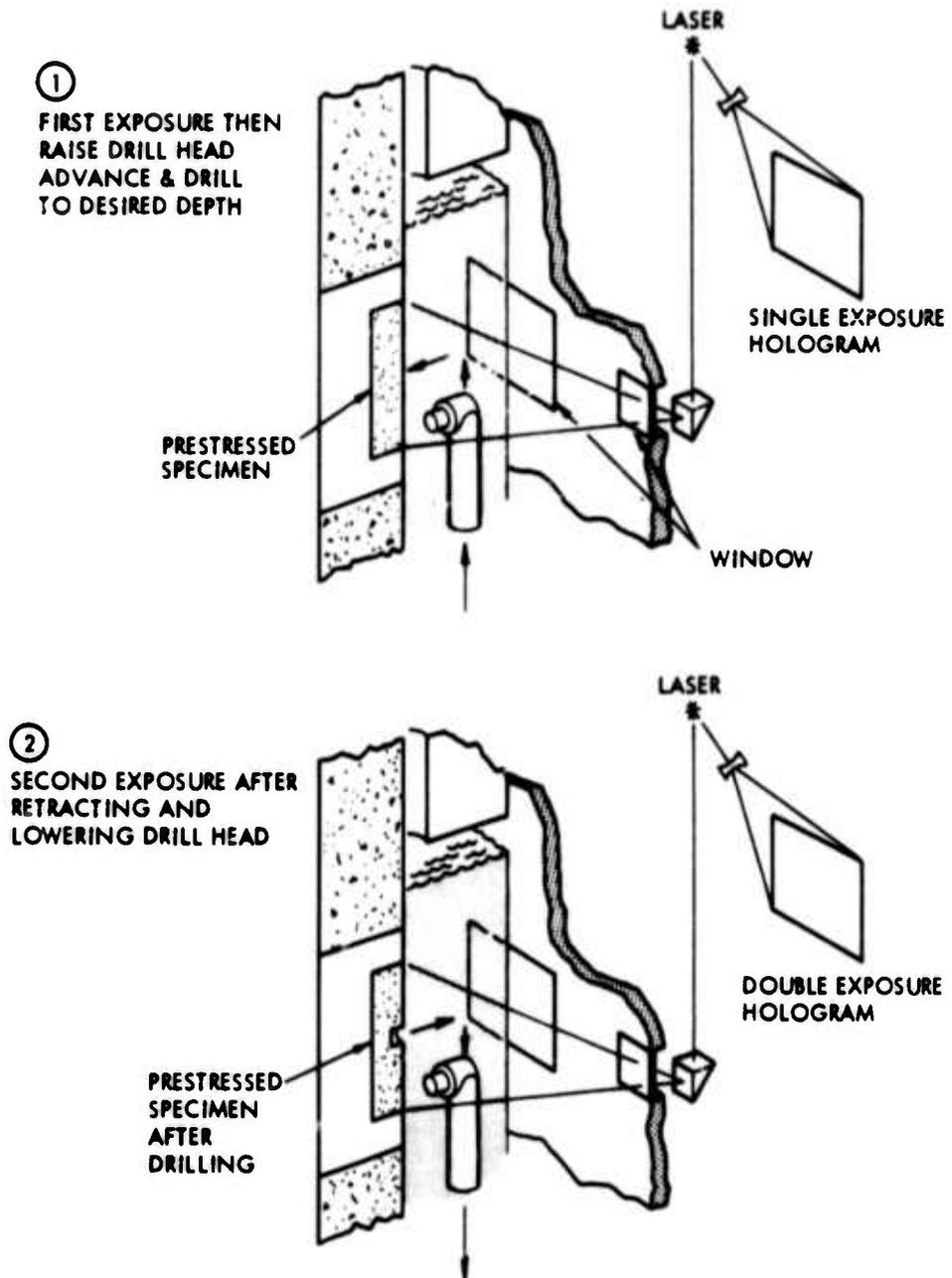
Figure 4.1: Double-exposure holographic procedure for drilling
prestressed specimens in a water-flooded simulated
borehole.

30

TRW

Figure 4.2: Summary table of hologram tests with prestressed specimens

Flat Specimen No.*	Side	Pre-Load (psi)	Drill Size (Inches)	Type of Hologram	Comments
1-R	A	4100	1/4	Double Exposure	No visible fringes.
	B	4100	1/4	Finite Fringe	No visible fringes
2-R	A	2000	1/4	Finite Fringe	Slight hint of displacement around hole with finite fringe background.
	B	2000	1/4	Double exposure	Part of one fringe formed near hole.
3-R	A	2800	1/4	Double Exposure	First indication of a single lobe fringe pattern superimposed on a slight nonoperator induced fringe pattern.
	B	2800	1/4	Double Exposure	First indication of a double lobe fringe pattern superimposed on a slight nonoperator induced fringe pattern.
4-R	A	4500	1/4	Finite Fringe	Low fringe contrast (too much displacement between exposures).
	B	4500	1/4	Double Exposure	Double lobe fringe pattern super-imposed on nonoperator induced fringe pattern.
5-R	A	3400	1/4	Finite Fringe	Weak indication of displacement around hole with finite fringe background.
	B	3400	1/4	Finite Fringe	No fringes (too much displacement between exposures).

31

Figure 4.2 (Cont'd.)

Flat Specimen No.*	Side	Pre-Load (psi)	Drill Size (Inches)	Type of Hologram	Comments
6-R	A	2700	1/4	Double Exposure	Small double lobe fringe pattern superimposed on a slight non-operator induced fringe pattern.
	B	2700	3/8	Finite Fringe	Indication of displacement around hole with finite fringe background (see Figure 4.8).
7-R	A	4200	3/8	Double Exposure	Double lobe fringe pattern superimposed on a moderate nonoperator induced fringe pattern (see Fig. 4.6)
	B	4200	3/8	Double Exposure	Tri-lobe fringe pattern superimposed on a slight nonoperator induced fringe pattern (see Figs. 4.3 & 4.4).
8-R	A	4500	3/8	Double Exposure	Tri-lobe fringe pattern very similar to 7-R:B except lower fringe contrast.
	B	4500	3/8	Finite Fringe	Finite fringe density too high to see effect around hole.
9-C	A	<2000	3/8	Double Exposure	No fringes (cloudy water).
	B	<2000	3/8	Finite Fringe	Slight indication of displacement around hole with finite fringe background.

*All rectangular (R) except No. 9 which was cylindrical (C).

relief than with the 1/4" drill. Photographs of several of these holograms are included to demonstrate results from the series of tests.

Two examples of strain relief fringe patterns obtained from the same double exposure hologram (7-R:B of Figure 4.2) of a flat rectangular pre-stressed granite specimen are shown in Figures 4.3 and 4.4. The only difference in the two photographs is the viewing angle of the camera behind the hologram. (The illumination and viewing geometry are discussed further in Section 6.3 and are shown schematically in Figure 4.5.) The viewing angle is close to the center line of the hologram axis in Figure 4.3. This view accentuates the lower lobe which is in direct compression while the lobe on the left is minimized. It should also be noted that no trace of drilling is observed since the first exposure of the specimen predominates over the second exposure. Likewise, no fringes appear in the center equal to the core diameter. The viewing angle for the photograph shown in Figure 4.4 maximized the two lobes giving an indication of the formation of a third lobe opposite the lower lobe which is in direct compression. A comparable double exposure hologram (7-R:A of Fig. 4.2) made from the other side of the same granite specimen is shown for comparison in Figure 4.6. The loading direction was the same in both cases while a greater nonoperator induced displacement due to drilling is observable in Figure 4.6 as a greater fringe density on the right side of the hole. The rigid body displacement fringes on the right in these two holograms were also encountered to a varying degree in other double exposure holograms.

The pre-load on the flat rectangular specimen shown in Figures 4.3, 4.4, and 4.6 was ≈ 4200 psi. These photographs were enlarged to approximately 1:1 magnification and are directly comparable to the computer generated fringe pattern, using well known solutions from the theory of elasticity, shown in Figure 4.7 and analyzed in Section 6.4. For comparison purposes, the corresponding fringe numbers are assigned to the photographs as well as the computer generated fringe patterns. Similarity in the experimentally obtained fringe patterns in Figures 4.3, 4.4 and 4.6 with those generated using a computer and theory of elasticity solutions is obvious. Differences which could result from simplifications in ana-lytical generation of fringe patterns are further discussed in Section 6.4.
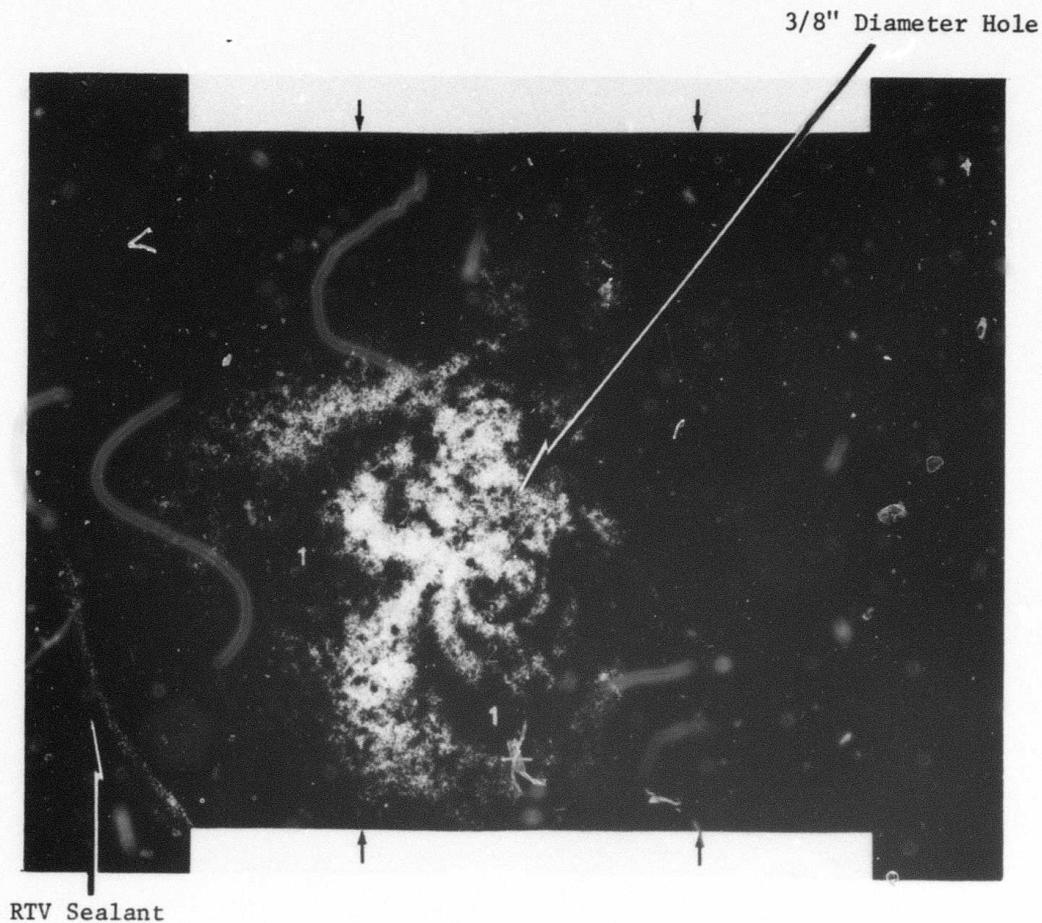
33

Figure 4.3: Full scale photograph (∿ 5.5 inch diameter in the
field of view) from double-exposure hologram
(7-R:B of Figure 4.2) of prestressed flat rectangular
specimen (White Sierra granite) with fixture shown
in Figure 3.9. The axis of loading is represented
by the two loading blocks in their approximate
position for the test. The preload, as measured with
a strain gage, was approximately 4200 psi. The
viewing direction was along the axis extending
outward from the 3/8" corehole.   (See Figure 4.4
for a different viewing angle of the hologram.)
Corresponding fringe numbers can be compared to the
computer generated fringes in Figure 4.7.
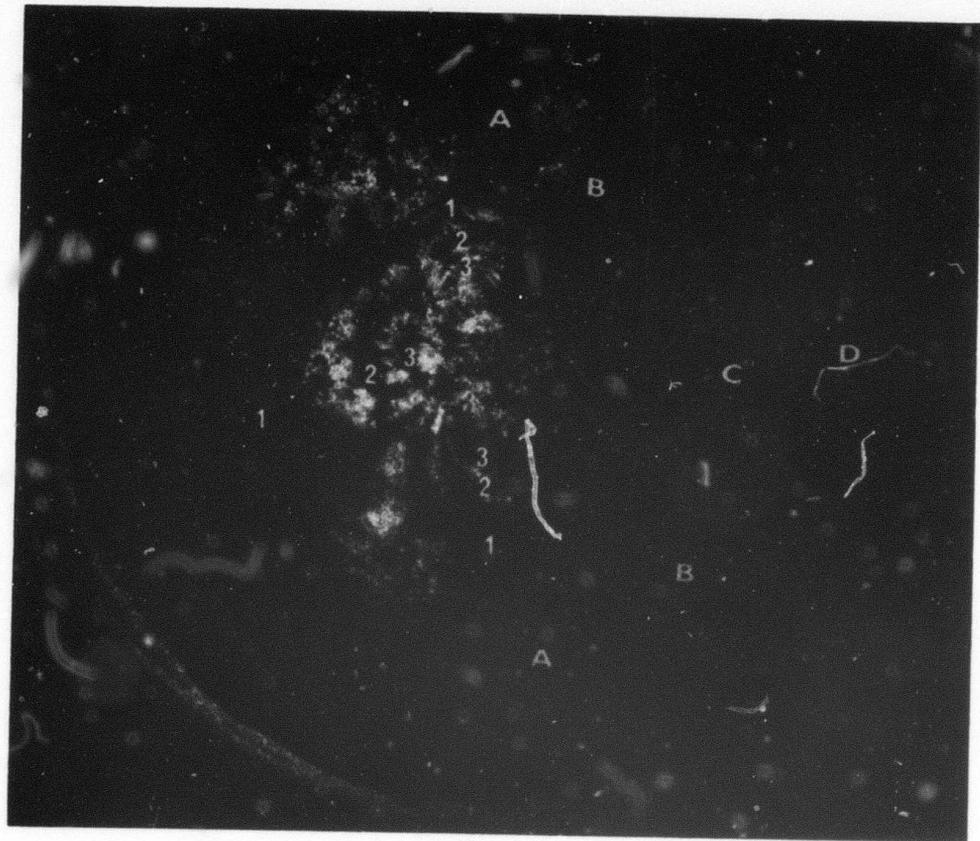
LOADING AXIS

Figure 4.4: Full scale photograph from the same double-exposure
hologram (7-R:B of Figure 4.2) as Figure 4.3. The
viewing direction was slightly off the axis
extending outward from the 3/8" corehole to
emphasize the symmetry of the lower and left hand
lobes. The trace of a third lobe can be distinguished
at the top. The broader fringes on the right in
this photograph, as well as Figure 4.3, are believed
due to an uninduced rigid body motion between
exposures. Fringes believed due to strain relief are
designated with numbers while fringes believed due
to rigid body motion are marked with letters.

Figure 4.5: Holographic geometry used to record and observe fringes on granite surface. NOTE: Loading of flat rectangular specimen was at 45° to this orientation.

LOADING AXIS

Figure 4.6: Full scale photograph from double-exposure hologram
(7-R:A of Figure 4.2). This hologram was made from
the opposite side of the specimen shown previously
in Figures 4.3 and 4.4 (7-R:B of Figure 4.2). Fringes
believed due to strain relief are designated with
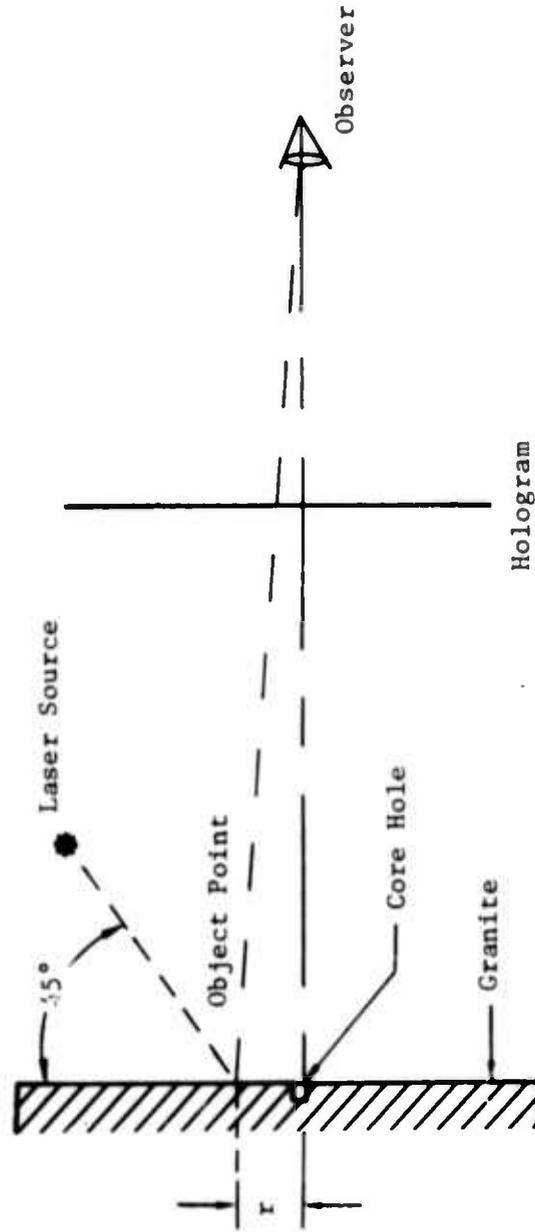numbers while fringes believed due to rigid body
motion are marked with letters.

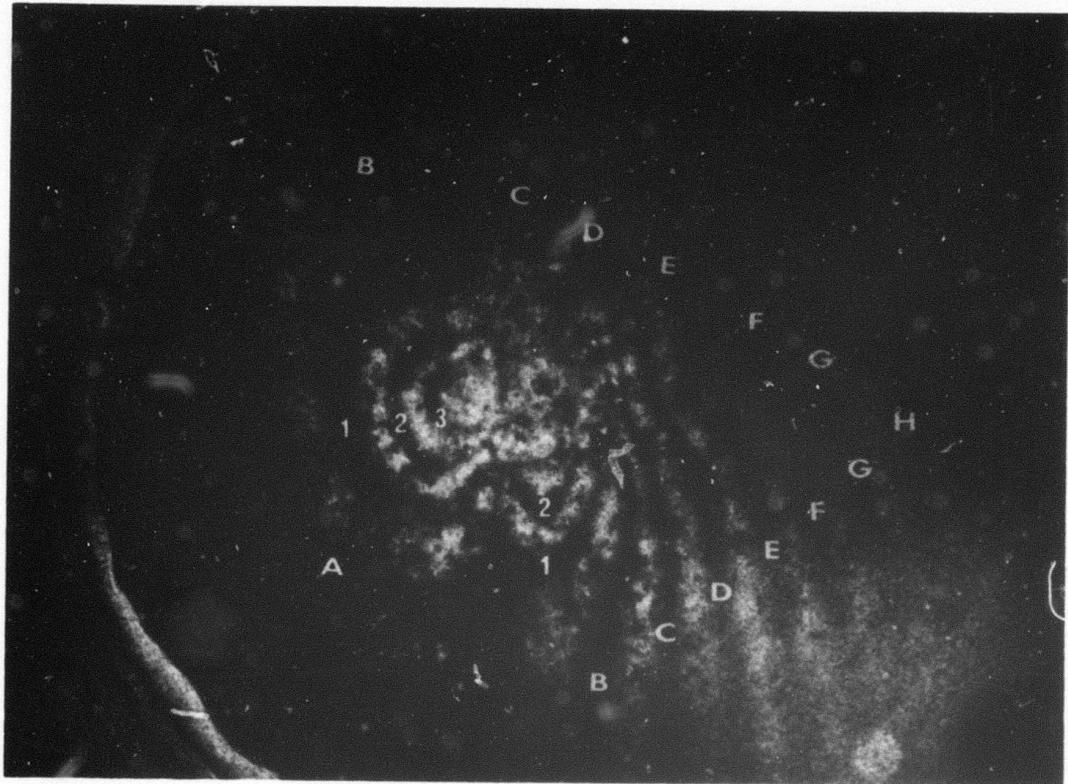# FRINGE PATTERNS FOR A UNIAXIALLY STRESSED HOLE
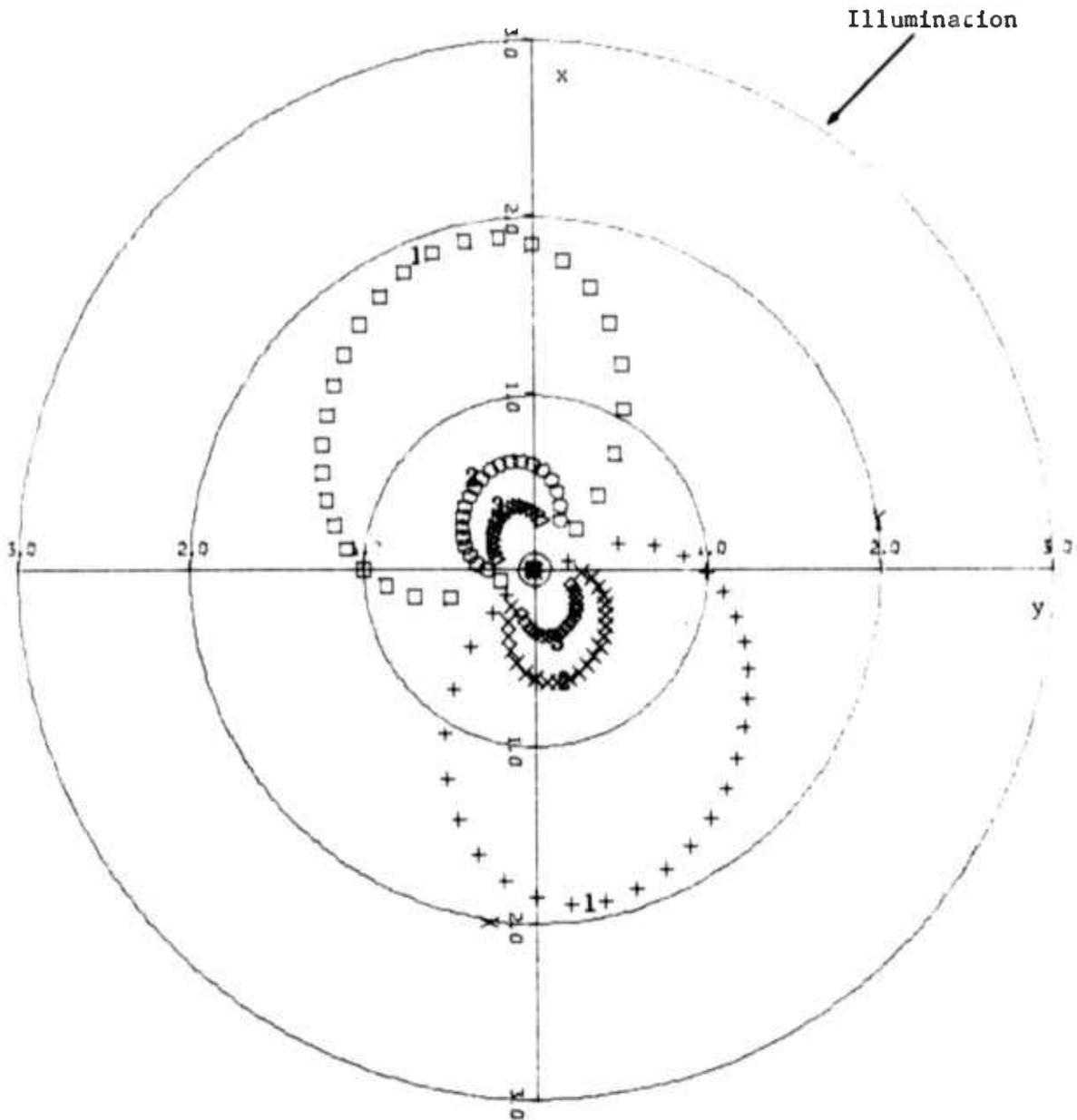
Figure 4.7: Full-scale (in inches) computer generated fringe pattern
with applied stress σ_0 = -4200 psi. The x-axis is the
loading axis used in the laboratory experiments.

TRW
SYSTEMS GROUP

An example of a strain relieved rock was obtained by finite fringe double exposure holographic interferometry and is shown in Figure 4.8 (6-R:B of Figure 4.2). Here approximatedly straight fringes were operator induced by a slight displacement of the rock specimen along the loading axis between exposures. It should be noted that this technique could have been equivalently accomplished by careful rotation of the hologram between exposures. These straight fringes are superimposed on the strain relieved area to yield a region of fringes curving inward toward the corehole. The effect of strain relief takes place in the region of departure from straight fringes. This technique was used to enhance strain relief at lower prestress levels.

3/8" Diameter Hole

LOADING AXIS

Figure 4.8: Full scale photograph from finite fringe double-exposure
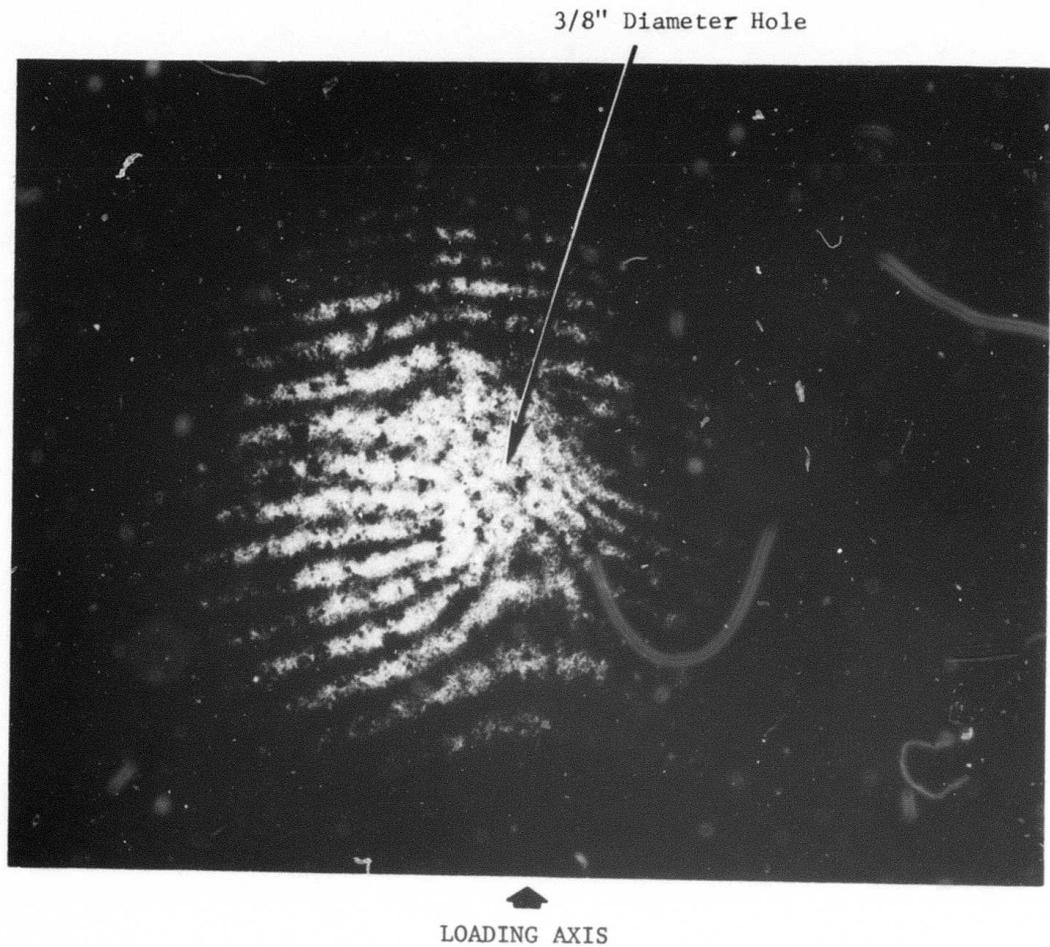hologram (6-R:B of Figure 4.2). The preload, as
measured with a strain gage, was approximately 2400 psi.
NOTE: The effect due to strain relief (i.e., departure
from straight fringes) is greater at the bottom.

5.0 ANALYTIC APPROACH FOR IN-SITU MEASUREMENTS

The ultimate objective of our development program is to design and construct a field instrument which is capable of measuring in-situ stress. We have to date demonstrated that holograms can be obtained in a water flooded environment and in a simulated borehole upon stress relieving around a side corehole. In the next phase of the development, we except to calculate the complete displacement field around the side corehole by modifying a computer code developed at TRW for determining displacements from holographic interferograms. The displacement field data and the elastic moduli of the rock formation will be utilized to obtain the values and orientation of the principal stresses in an arbitrary configuration taking into account the main borehole effect on the in-situ stress. The TRW computer program can be modified to incorporate the cylindrical geometry of the borehole and calculate the displacement field at several points along the wall in three dimensions.

The displacements at points on the borehole wall will then be used in conjunction with a finite element computer analysis to determine the in-situ stresses in the surrounding rock. An outline of how this analysis would proceed and the assumptions involved is included in the following pages. After this approach was developed, we became aware of related work in this area by Hirmatsu and Oka (Ref. 8). Time restraints have not permitted a detailed comparison of our results with those of Reference 8, but such a comparison would be performed in the early phases of any subsequent development.

The following sections of the report document the proposed approach which has been developed to determine in-situ stresses within the earth from holographic displacement measurements. The method involves drilling three small side holes in the wall of the 9 inch diameter corehole. Displacements are to be measured around each small side hole using the holographic apparatus. From these displacements a set of local stresses around a shallow hole in a half-space will be determined. These local stresses will be transformed analytically and then used in conjunction with the theory of stress concentration around a hole. Using this well developed theory, the far field stresses (away from the corehole)

can be determined. The objective of this section is to present a fairly detailed outline of the approach and the assumptions involved, thereby indicating the direction intended in future work.

5.1 Effect of the Corehole

Consider a corehole, of diameter D, drilled deep into the earth (Figure 5.1). By deep, we mean that the depth, h, in Figure 5.1 is several hundred times the diameter, D. Thus, the deep hole may be treated as infintely long (i.e., "deep") for purposes of stress analysis. Now define a cylindrical coordinate system (Z, R, ψ) - called the "Global" coordinate system - with the Z-axis oriented along the axis of the corehole.

Prior to drilling the corehole into the earth, at any depth we have a completely general stress field, denoted by Σ_{ij}. The symmetric tensor Σ_{ij} has six components, which we wish to determine as a function of depth, Z, in the earth. Another way of representing Σ_{ij} is in terms of three principal stresses Σ_1, Σ_2, Σ_3, and three principal directions (e.g., angles λ_1, λ_2, and λ_3). However, in either case, the stress tensor Σ involves <u>six</u> quantities which must be determined. This fact tells us that the holographic system must provide at least <u>six inde-</u><u>pendent</u> pieces of data from which we will then determine the six components of the in-situ stress tensor, Σ.

Clearly, it makes very little difference if we determine the in-situ stresses Σ in a particular coordinate system (e.g., Z, R, ψ) or not, since we have available to us well-known tensor transformations which allow us to transform the stress tensor to other coordinates. For example, if principal stresses are of primary interest, we can first find the stresses in the (Z, R, ψ) coordinate system and then diagonalize the stress tensor to find Σ_1, Σ_2, Σ_3, and their directions.

Thus, returning to Figure 5.1, we can now confine our attention to finding the six stress components (call them σ_{RR}, σ_{RZ}, σ_{ZZ}, $\sigma_{\psi\psi}$, $\sigma_{R\psi}$, $\sigma_{Z\psi}$) in the (Z, R, ψ) coordinates. We would like to find out what the six σ_{ij} values were (prior to drilling the corehole) in the in-situ rock. The presence of the corehole complicates our task somewhat, since it

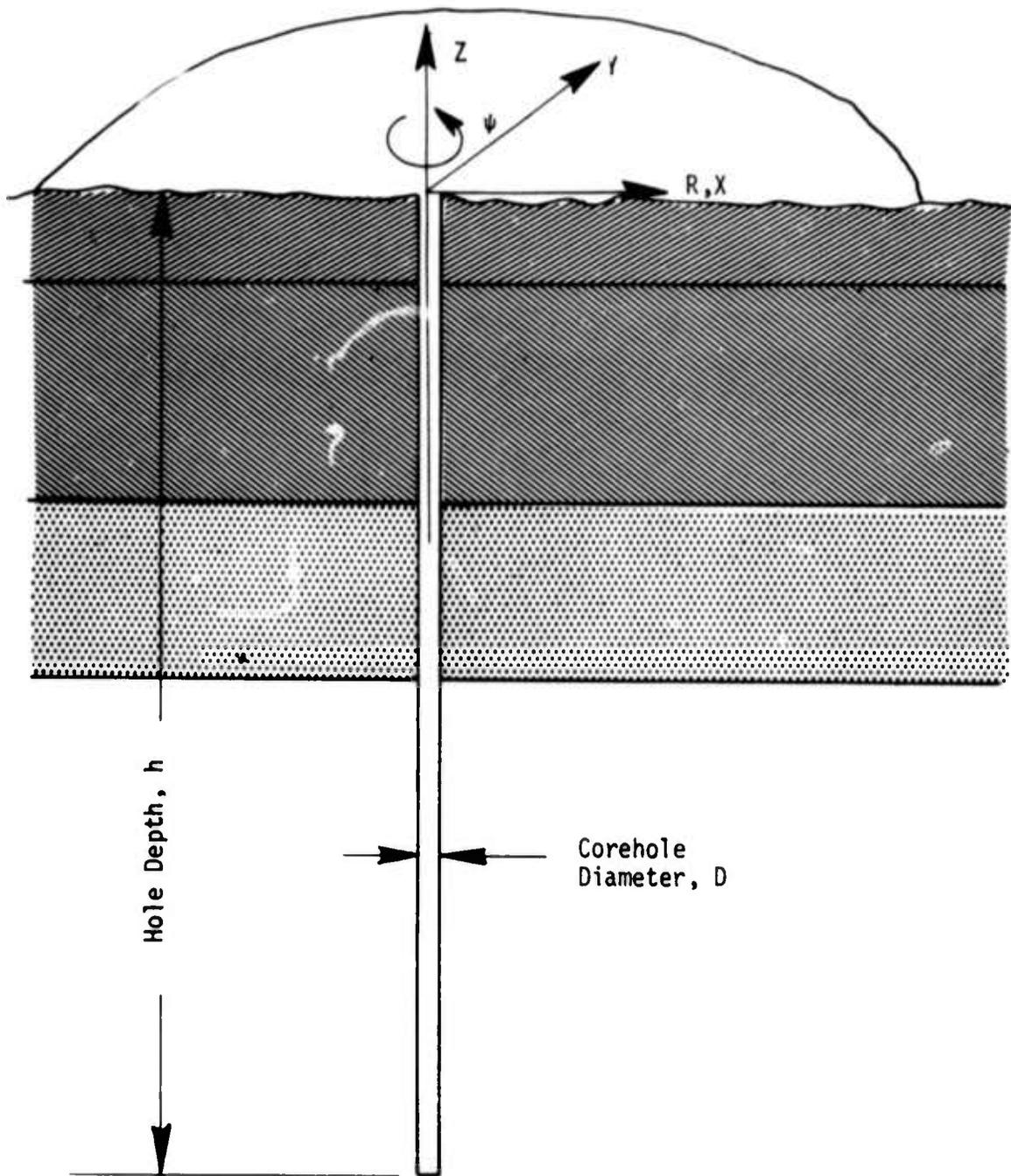Figure 5.1: Sketch of deep corehole and Global coordinates (Z, R, ψ).

causes local perturbations (commonly termed stress concentrations) in the stress field σ_{ij}. However, it is important to note that the stress components σ_{ZZ}, σ_{RZ}, and $\sigma_{Z\psi}$ are assumed <u>undisturbed</u> by the presence of the corehole. Since it is very deep (i.e., infinitely long) the corehole causes stress concentration effects only <u>perpendicular</u> to its axis and thereby disturbs just σ_{RR}, $\sigma_{\psi\psi}$, and $\sigma_{R\psi}$.

5.2 Use of the Side Holes

In order to determine the six σ_{ij} in (Z, R, ψ) coordinates, we begin by drilling a small side hole, of diameter d, in the wall of the core-hole. Referring to Figure 5.2, we have a view looking down along the Z-axis of the corehole. The small side hole has a depth denoted by e in Figure 5.2. Also illustrated schematically in Figure 5.2 is the stress concentration effect of the large hole, D.

A basic assumption at this point is that the side-hole diameter d is much less than the corehole diameter, D. That is,

$$\frac{d}{D} \ll 1 \tag{5.1}$$

The reason for this assumption is that stress concentration due to the corehole varies with the angle ψ. We wish to "sample" the stress field with our side hole, but we want our sample to be at a particular <u>point</u> in the circumferential angle, ψ. The side hole really samples over a width d out of a total possible length πD of the circumference. Thus, we want

$$\frac{\text{Sample Width}}{\text{Circumference}} = \frac{d}{\pi D} \ll 1 \tag{5.2}$$

For a uniform stress at infinity, given by

$$\left. \begin{array}{rcl} \sigma_X &=& \sigma \\[1mm] \sigma_Y &=& 0 \\[1mm] \sigma_{XY} &=& 0 \end{array} \right\} \quad \text{as } R \to \infty$$
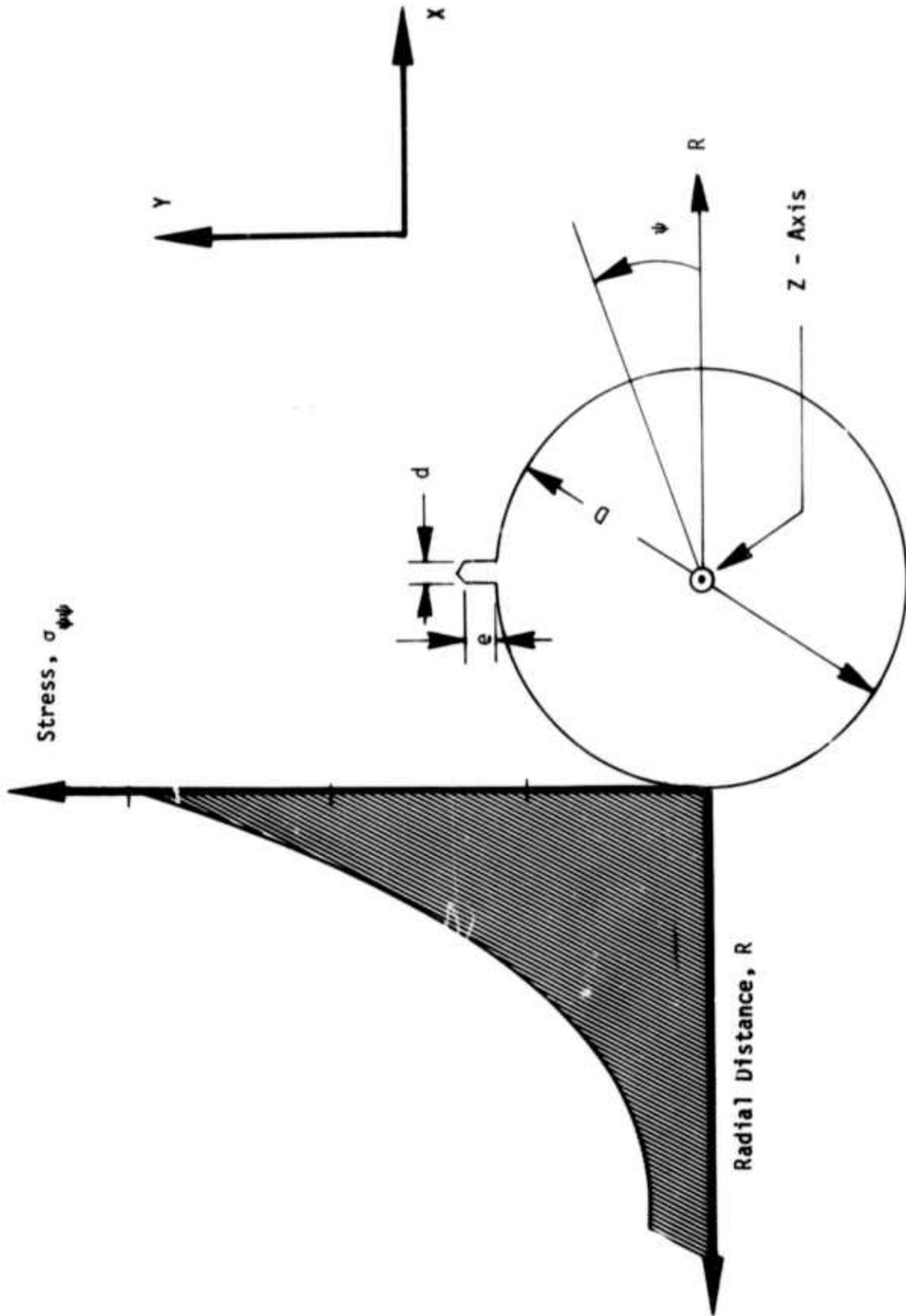
Figure 5.2: Sketch of side hole (diameter d, depth e) and stress concentration from corehole.

(where $X = R \cos \psi$

$\qquad Y = R \sin \psi$

are rectangular coordinates),

the stress field around the corehole is given by

$$\sigma_{RR} = \frac{\sigma}{2} \left[\left(1 - \frac{R_i^2}{R^2}\right) + \left(1 - \frac{4R_i^2}{R^2} + \frac{3R_i^4}{R^4}\right) \cos 2\psi \right] \qquad (5.3)$$

$$\sigma_{\psi\psi} = \frac{\sigma}{2} \left[\left(1 + \frac{R_i^2}{R^2}\right) - \left(1 + \frac{3R_i^4}{R^4}\right) \cos 2\psi \right] \qquad (5.4)$$

$$\sigma_{R\psi} = -\frac{\sigma}{2} \left[1 + \frac{2R_i^2}{R^2} - \frac{3R_i^4}{R^4} \right] \sin 2\psi \qquad (5.5)$$

where R_i is the radius of the corehole.

When sampling this stress field with a side hole of diameter d, we will have a stress variation $\Delta\sigma$ across the distance d. To estimate $\Delta\sigma$ we have

$$\Delta\sigma_{\psi\psi} = \frac{1}{R} \left.\frac{\partial \sigma_{\psi\psi}}{\partial \psi}\right|_{R_i} (d)$$

$$\Delta\sigma_{\psi\psi} = \frac{d}{R_i} \left(\frac{\sigma}{2}\right) 2 \left[(1 + 3) \sin 2\psi\right] \qquad (5.6)$$

and the percent variation in $\sigma_{\psi\psi}$ is

$$\frac{\Delta\sigma_{\psi\psi}}{\sigma_{\psi\psi}} = \frac{\frac{d}{R_i} \left(\frac{\sigma}{2}\right) 8 \sin 2\psi}{\left(\frac{\sigma}{2}\right) 2 \left[1 - 2 \cos 2\psi\right]} = \frac{\frac{4d}{R_i} \sin 2\psi}{\left[1 - 2 \cos 2\psi\right]} \qquad (5.7)$$

Since $\sigma_{\psi\psi}$ can go to zero at the angle $2\psi_o = \cos^{-1}\frac{1}{2}$ on the circumference, large percentage variations $\frac{\Delta\sigma}{\sigma}$ may occur. However, the effect can be minimized by making the quantity

$$\frac{4d}{R_i} \ll 1 \tag{5.8}$$

which is more stringent than the inequality assumed in Eq. (5.1)

$$\frac{d}{D} = \frac{d}{2R_i} \ll 1$$

given previously. The preceding discussion makes quite clear the requirement that the side-hole diameter should be kept small.

As regards the depth, e, of the side hole, we again want to make it sufficiently "shallow" such that

$$\frac{\text{Depth of Sidehole}}{\text{Radius of Corehole}} = \frac{e}{R_i} \ll 1 \tag{5.9}$$

for reasons similar to those just presented. That is, we want the side hole to "sample" (i.e., to "average") the stress $\sigma_{\psi\psi}$ over a rather short penetration de   . Consider the case $2\psi = \pi$ (i.e., $\psi = 90°$) in Equation (5.4). Then at the inside surface of the corehole we have

$$\sigma_{\psi\psi} = 3\sigma \begin{cases} R = R_i \\ \psi = 90° \end{cases} \tag{5.10}$$

Now let $e = \varepsilon R_i$, where ε is the side-hole depth, as a fraction of the corehole radius, R_i. At the bottom of the side hole, we have

$$R = R_i + e = R_i(1 + \varepsilon) \tag{5.11}$$

47

Substituting this expression for R in Equation (5.4) and expanding in powers of the small parameter ε gives

$$\sigma_{\psi\psi} = (3 - 7\varepsilon)\sigma \left\{ \begin{array}{l} R = R_i\ (1 + \varepsilon) \\ \psi = 90° \end{array} \right. \tag{5.12}$$

at the bottom of the side hole.

To obtain a feel for the values of $\frac{d}{D}$ and $\varepsilon = \frac{e}{R_i}$, consider a 9 inch diameter corehole with a small side hole that is 1/4 inch in diameter and 1/4-inch deep:

Then

$$\frac{d}{D} = \frac{1/4}{9} = \frac{1}{36} \ll 1$$

and

$$\varepsilon = \frac{1/4}{9/2} = \frac{1}{18} \ll 1$$

which are felt to be sufficiently small for most purposes.

5.3 Analysis of the Side Hole

When d/D and ε of the preceding section are small enough, the problem of the side-hole can be idealized as a shallow hole in a stressed half-space, Figure 5.3. To orient the reader, the half-space has a local coordinate system (r, θ, z) where the local z-axis is in the radial direction, R, of the (Z, R, ψ) corehole coordinate system. In other words, the half-space represents the wall of the corehole, and the side hole is drilled in the radial direction, R, of the corehole. By keeping the ratio

$$\frac{d}{D} \ll 1$$

small, it is assumed that the curvature of the corehole wall can be neglected and the side hole can then be analyzed as having been drilled into a stressed half-space.
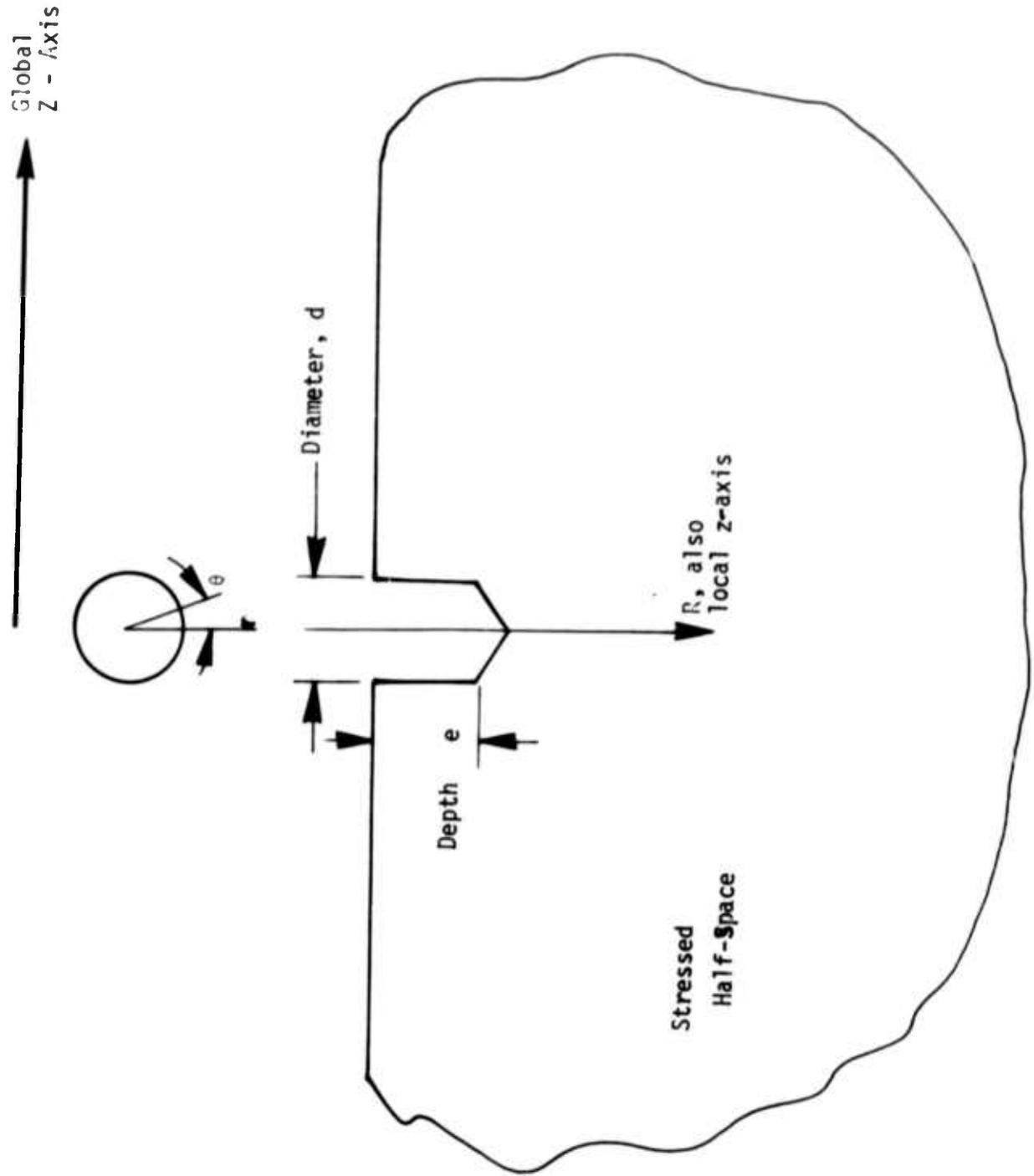
48

Global
Z - Axis

Diameter, d

θ

R, also
local z-axis

Depth   e

Stressed
Half-Space

Figure 5.3:   Drilled hole in a stressed half-space.

49

The local stresses in the half-space σ_{rr}, $\sigma_{r\theta}$, and $\sigma_{\theta\theta}$ (in r, θ, z coordinates) are clearly related to the stresses $\sigma_{\psi\psi}$, σ_{ZZ}, $\sigma_{\psi Z}$, and σ_{RZ} of the corehole coordinates (Z, R, ψ). If the location of the first side hole is denoted by $\psi = 0$, then stresses σ_{ZZ}, $\sigma_{\psi\psi}$, and $\sigma_{Z\psi}$ are acting in the wall of the corehole. The other stresses σ_{RR}, $\sigma_{R\psi}$, and σ_{RZ} are zero since the wall of the corehole is a free surface.

Now suppose that the local x-axis ($\theta = 0$) is oriented in the direction of decreasing ψ. Then the relationship between the stress components is

$$\overset{\circ}{\sigma}_{rr} = \sigma_{\psi\psi} = \overset{\circ}{\sigma}_{xx}$$

$$\overset{\circ}{\sigma}_{\theta\theta} = \sigma_{ZZ} = \overset{\circ}{\sigma}_{yy} \qquad (5.13)$$

$$\overset{\circ}{\sigma}_{r\theta} = \sigma_{Z\psi} = \overset{\circ}{\sigma}_{xy}$$

for the pre-stress values in the half-space well away from the side-hole. (We have added a local x, y, z coordinate system coincident with the local r, θ, z coordinates. As usual, we have $x = r \cos \theta$, $y = r \sin \theta$, etc.) The zero superscripts on the stresses in Equations (5.13) are used to denote that these values apply well away from the side hole. Equations (5.13) thus denote stresses which are not influenced by the presence of the side hole.

5.4 Fundamental Problem for the Half-Space

The pre-stress values $\overset{\circ}{\sigma}_{xx}$, $\overset{\circ}{\sigma}_{yy}$, and $\overset{\circ}{\sigma}_{xy}$ (which arise from the stresses $\sigma_{\psi\psi}$, σ_{ZZ}, and $\sigma_{Z\psi}$) will cause nonuniform distortions (e.g., elliptical distortions) around the side-hole. The problem we have is an initially stressed half-space into which a small, shallow hole is drilled. Since we are employing linear elasticity theory throughout this discussion, the principle of superposition is available to us, and we need consider only one fundamental elasticity problem for the half-space.

The problem to be analyzed is a half-space with single prestress at infinity, i.e.,

$$\left.\begin{array}{rcl} \overset{\circ}{\sigma}_{xx} &=& \sigma \\\\ \overset{\circ}{\sigma}_{yy} &=& 0 \\\\ \overset{\circ}{\sigma}_{xy} &=& 0 \end{array}\right\} \quad \text{as } r \to \infty \qquad (5.14)$$

far away from the origin.

The solution of this problem in polar coordinates involves displacements of the form

$$u = U_o(r) + U_2(r) \cos 2\theta$$

$$v = V_o(r) \sin 2\theta \qquad\qquad (5.15)$$

$$w = W_o(r) + W_2(r) \cos 2\theta$$

which can be determined by a finite-element computer program.

By a transformation of coordinates, namely, $\theta' = \theta + \pi/2$, we can transform the solution (5.15) to obtain the solution for the prestress condition

$$\left.\begin{array}{rcl} \overset{\circ}{\sigma}_{xx} &=& 0 \\\\ \overset{\circ}{\sigma}_{yy} &=& \sigma \\\\ \overset{\circ}{\sigma}_{xy} &=& 0 \end{array}\right\} \quad \text{as } r \to \infty \qquad (5.16)$$

namely, prestress in the y-direction.

51

Finally, by superimposing the preceding two solutions and then using the transformation $\theta' = \theta + \pi/4$ we can transform the solution (5.15) to obtain pure-shear at infinity:

$$\left.\begin{aligned} \overset{\circ}{\sigma}_{xx} &= 0 \\[1em] \overset{\circ}{\sigma}_{yy} &= 0 \\[1em] \overset{\circ}{\sigma}_{xy} &= \sigma \end{aligned}\right\} \quad \text{as } r \to \infty \qquad (5.17)$$

The general case, represented by Equation (5.13) involves the three prestress values $\overset{\circ}{\sigma}_{xx}$, $\overset{\circ}{\sigma}_{yy}$, and $\overset{\circ}{\sigma}_{xy}$ and can be written as the superposition of three solutions of the form (5.15) for the displacements u, v, and w. That is, we can write

$$\left.\begin{aligned} u_{TOTAL} &= u_1 \overset{\circ}{\sigma}_{xx} + u_2 \overset{\circ}{\sigma}_{yy} + u_3 \overset{\circ}{\sigma}_{xy} \\[1em] v_{TOTAL} &= v_1 \overset{\circ}{\sigma}_{xx} + v_2 \overset{\circ}{\sigma}_{yy} + v_3 \overset{\circ}{\sigma}_{xy} \\[1em] w_{TOTAL} &= w_1 \overset{\circ}{\sigma}_{xx} + w_2 \overset{\circ}{\sigma}_{yy} + w_3 \overset{\circ}{\sigma}_{xy} \end{aligned}\right\} \qquad (5.18)$$

where (u_1, v_1, w_1) are displacements resulting from a unit value of $\overset{\circ}{\sigma}_{xx}$ applied alone at infinity

            (u_2, v_2, w_2) result from a unit value of $\overset{\circ}{\sigma}_{yy}$ applied alone at infinity

            (u_3, v_3, w_3) result from a unit value of $\overset{\circ}{\sigma}_{xy}$ applied alone at infinity

TRW

5.5 Use of the Displacement Measurements

By measuring the displacements u, v and w at three locations around the side hole, we can determine the values of σ_{xx}°, σ_{yy}° and σ_{xv}° which are superposition constants in Equations (5.18). In actual practice, we expect to have holographic displacement data at many locations on the wall surface around the side hole, and a least-squares procedure can be used to find the "best fit" values for σ_{xx}°, σ_{yy}° and σ_{xy}°; i.e., the prestress values around the side-hole.

Having found the pre-stress values from the holographic data, we have from Equation (5.13) given previously

$$\left.\begin{aligned} \sigma_{\psi\psi} &= \sigma_{xx}^{\circ} \\ \sigma_{zz} &= \sigma_{yy}^{\circ} \\ \sigma_{z\psi} &= \sigma_{xy}^{\circ} \end{aligned}\right\} \tag{5.19}$$

for three of the stress components in the global (Z, R, X) coordinate system. Thus, at this point, we have found the stresses σ_{zz} and σ_{zx} (which are not affected by the presence of the corehole) and which therefore represent the prestress values

$$\left.\begin{aligned} \sigma_{zz} &= \sigma_{yy}^{\circ} = \sigma_{zz} \\ \sigma_{z\psi} &= \sigma_{xy}^{\circ} = \sigma_{zy} \end{aligned}\right\} \tag{5.20}$$

where we have added a rectangular coordinate system (X, Y, Z) coincident with the cylindrical coordinates (R, ψ, Z) discussed previously, (see Figure 5.1). Accordingly, we have found two of the six components of the in-situ stress tensor Σ which we originally set out to determine. The other stress components require that we make additional measurements on other side holes, as discussed in the sections which follow.

5.6 Use of a Second Side Hole

The first side-hole serves to fix the location of the X-axis (i.e., $\psi = 0$) in our corehole coordinate system. Now suppose we rotate the apparatus 90° and drill a second side hole at $\psi = 90°$, i.e., along the direction of the Y-axis. Again we locate a local coordinate system (r, θ, z) or (x, y, z) with the local z-axis aligned with the side hole, and the local x-axis in the direction of decreasing ψ. Then the relationship between the stress components is again given by Equations (5.13) and we can again apply superposition principles as discussed relative to Equations (5.14) through (5.18).

From the displacement measurements around the second side-hole, we can determine a second set of prestress values similar to those found previously. Thus, for the second side hole we have

$$\left.\begin{array}{c} \sigma_{\psi\psi} = \overset{\circ}{\sigma}_{xx} \\[2ex] \sigma_{zz} = \overset{\circ}{\sigma}_{yy} \\[2ex] \text{and} \quad \sigma_{z\psi} = \overset{\circ}{\sigma}_{xy} \end{array}\right\} \tag{5.21}$$

as for the previous case.

Using Equations (5 21) and the fact that the second side hole is oriented along the Y-axis ($\psi = 90°$) we have determined another component of the in-situ stress tensor, namely

$$\sigma_{z\psi} = \overset{\circ}{\sigma}_{xy} = \sigma_{zx} \tag{5.22}$$

At the same time, we have a second measurement of the axial stress, σ_{zz}, from

$$\sigma_{zz} = \overset{\circ}{\sigma}_{yy} = \sigma_{zz} \tag{5.23}$$

5.7 Requirements for a Third Side Hole

In the preceding discussion we have said very little about the tangential stress, $\sigma_{\psi\psi}$. From the two side holes (at $\psi = 0$ and $\psi = 90°$) we will have two different values for $\sigma_{\psi\psi}$. Call them

$$\overset{1}{\sigma}_{\psi\psi} \text{ (from the first side hole)}$$

and

$$\overset{2}{\sigma}_{\psi\psi} \text{ (from the second side hole)}$$

By making measurements around a third side hole and finding $\overset{3}{\sigma}_{\psi\psi}$ we can then in principle solve three equations in three unknowns to find the remaining three in-situ stress components.

For example, suppose we drill the third side hole at $\psi = 45°$ (Figure 5.4). Now, referring to Figure 5.4, we have a stress concentration problem in two-dimensions (R, ψ) which is centered on the corehole (Z-axis). Furthermore, we have measured the tangential stress $\sigma_{\psi\psi}$ at three locations, and we wish to find the far-field stresses σ_{XX}, σ_{YY}, and σ_{XY}. By the principle of superposition, we can write three equations of the form

$$
\begin{aligned}
\overset{1}{\sigma}_{\psi\psi} &= \alpha_{11}\,\sigma_{XX} + \alpha_{12}\,\sigma_{YY} + \alpha_{13}\,\sigma_{XY} \\[2ex]
\overset{2}{\sigma}_{\psi\psi} &= \alpha_{21}\,\sigma_{XX} + \alpha_{22}\,\sigma_{YY} + \alpha_{23}\,\sigma_{XY} \\[2ex]
\overset{3}{\sigma}_{\psi\psi} &= \alpha_{31}\,\sigma_{XX} + \alpha_{32}\,\sigma_{YY} + \alpha_{33}\,\sigma_{XY}
\end{aligned}
\tag{5.24}
$$

where the coefficient α_{11} relates the tangential stress at $\psi = 0$ to a uniform field σ_{XX} at infinity, α_{32} relates the tangential stress at $\psi = 45°$ to a uniform field σ_{YY} at infinity, etc.
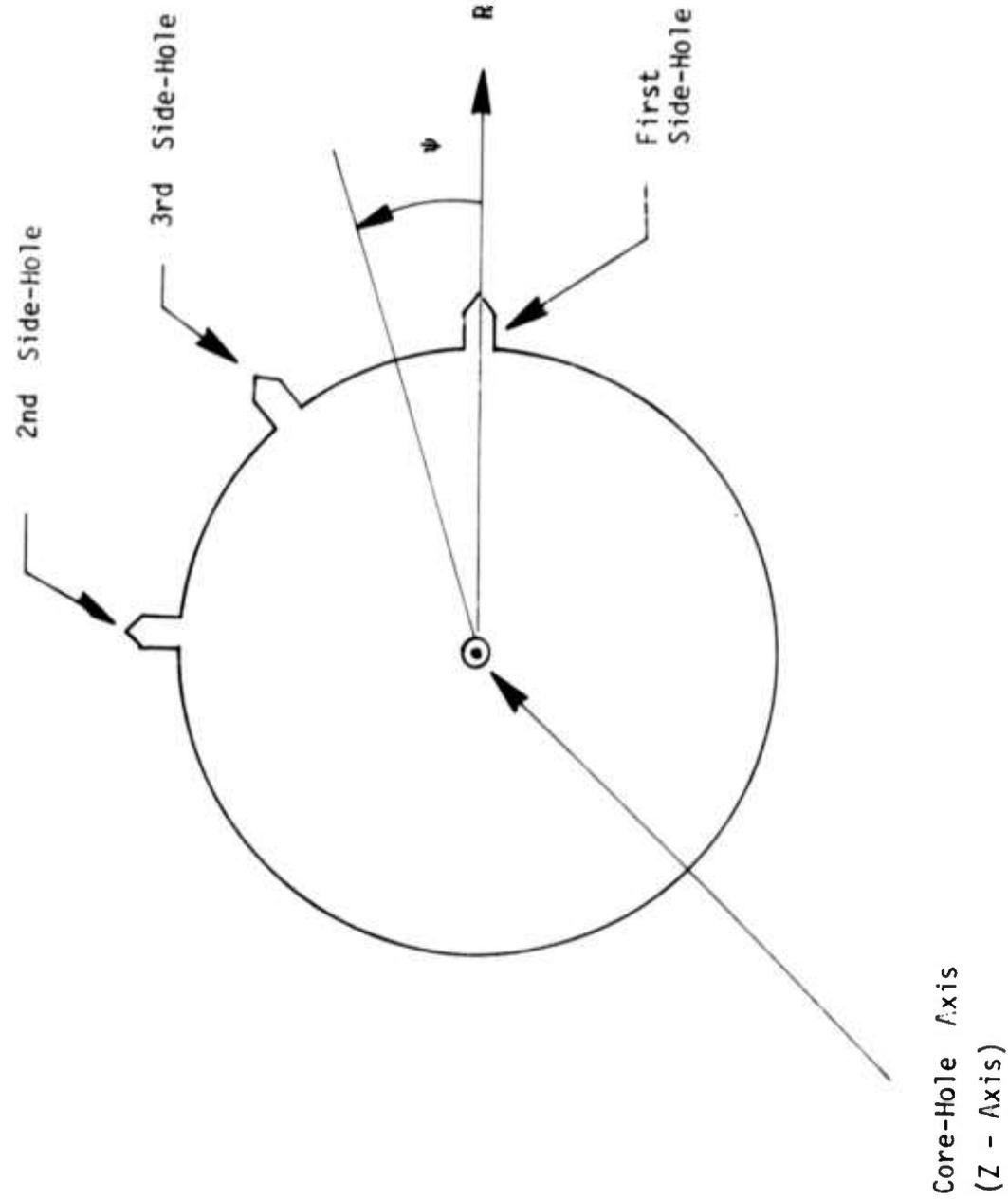
Figure 5.4: Sketch of three side holes.

The Equations (5.24) can be written in matrix fcrm

$$\vec{\sigma}_{\psi\psi} \ = \ [\alpha] \ \vec{\sigma} \tag{5.25}$$

and the coefficient matrix then inverted to yield the remaining three desired stress components:

$$\left\{ \begin{array}{c} \sigma_{XX} \\ \sigma_{XY} \\ \sigma_{YY} \end{array} \right\} \ = \ [\alpha]^{-1} \ \left\{ \begin{array}{c} \sigma_{\psi\psi}^{1} \\ \sigma_{\psi\psi}^{2} \\ \sigma_{\psi\psi}^{3} \end{array} \right\} \tag{5.26}$$

5.8 Alternate Locations for the Side Holes

The method just outlined is oriented toward determining the six components of the in-situ stress tensor in a relatively straightforward manner. Practical considerations may dictate that the side holes cannot be drilled at $\psi = 0$, $45°$, and $90°$, and therefore it is worthwhile to consider alternate drilling schemes.

One alternative would be to drill the three side holes at intervals of $120°$. This approach requires that the holographic device be capable of larger angular excursions, and the design may be more complicated as a result. In addition, the analysis of the results is slightly more complicated than that presented herein when the stress field is sampled at $120°$ intervals.

An alternate scheme, which may provide slightly less accurate results is to drill the side holes at $\psi = 0$, $22.5°$, and $45°$. For this set of holes, the matrix Equation (5.26) is expected to have a slightly poorer inverse which may generate slightly larger errors in the stress components. Furthermore, it is clear that a choice of three closely-spaced side holes (e.g., 0, $5°$, $10°$) is inappropriate since the problem is expected to be very poorly conditioned in this latter case.

In addition, three closely spaced side holes can be expected to interact strongly with one another and no longer each behave as a single hole in an elastic half-space. Recall that our analysis assumes a small diameter side hole d in a large diameter corehole, D. If the hole spacing s, in the circumferential direction is not several times greater than the side-hole diameter d, then the assumption of a single hole in an elastic half-space loses its validity. For this reason, it is recommended that the side holes be drilled at $\psi = 0$, 45°, and 90° if possible and certainly not closer than $\psi = 0$, 22.5°, and 45°.

TRW
SYSTEMS GROUP

6.0 COMPUTER GENERATION OF FRINGE PATTERNS
     FOR LABORATORY EXPERIMENTS

The rectangular specimen was chosen primarily on the basis that the stress level could be readily controlled and sufficient stress applied to provide several fringes on the interferogram. As a consequence, the analysis of the rectangular specimen required certain simplifying assumptions many of which would not have been necessary for the cylindrical specimen. Nevertheless, the theoretical fringe patterns computed using these assumptions bear a very close resemblance to those measured experimentally for the rectangular specimen.

Two main avenues of approach were available in the analysis of the rock specimens. One approach was to record the experimental fringe pattern and from it then determine the corresponding displacement field $\Delta\vec{u}(x,y,z)$ as a function of space on the rock surface. Then by differentiating the displacement field and performing other analysis, the strain field $\epsilon_{ij}(x,y,z)$ and the stress field $\sigma_{ij}(x,y,z)$ in the rock would be determined. The stress field thus determined from the holographic data would then be compared with the applied stress field (which had been measured independently by other means such as strain gages).

The approach just described is the most satisfying one, but it is also more costly and time-consuming that the second alternative. In the second approach, one makes the assumption that the stress and displacement fields are known, and then the corresponding (theoretical) interference fringe pattern is calculated. If the calculated fringe pattern "looks like" the experimental pattern, it is safe to assume that the known (theoretical) stress field is quite close to the stress field which was present in the experiment.

With regard to the first approach, TRW has developed a general analysis procedure and a corresponding computer program for calculating surface displacements from experimental interferograms. This program was developed in the performance of other related holographic work and not on the present contract. Using this program, it is possible to take an interferogram (such as Figure 4.4, for example) and compute the associated surface

59

displacements. This program requires a knowledge of the fringe order, n, and requires that the location of each fringe be measured as a function of (x,y) coordinates on the surface of the body.

Although this procedure of deducing displacements (and then deriving strains) from interferograms has been used previously (Ref. 9) constraints of time and money would not permit its use on the present contract. Consequently, the simpler alternative of computing a "theoretical" fringe pattern corresponding to a known stress field was used herein. The similarity between the computed fringe pattern and the experimental fringe pattern is quite good, as will become apparent from subsequent discussion and figures.

6.1 Discussion of the Assumed Stress Field

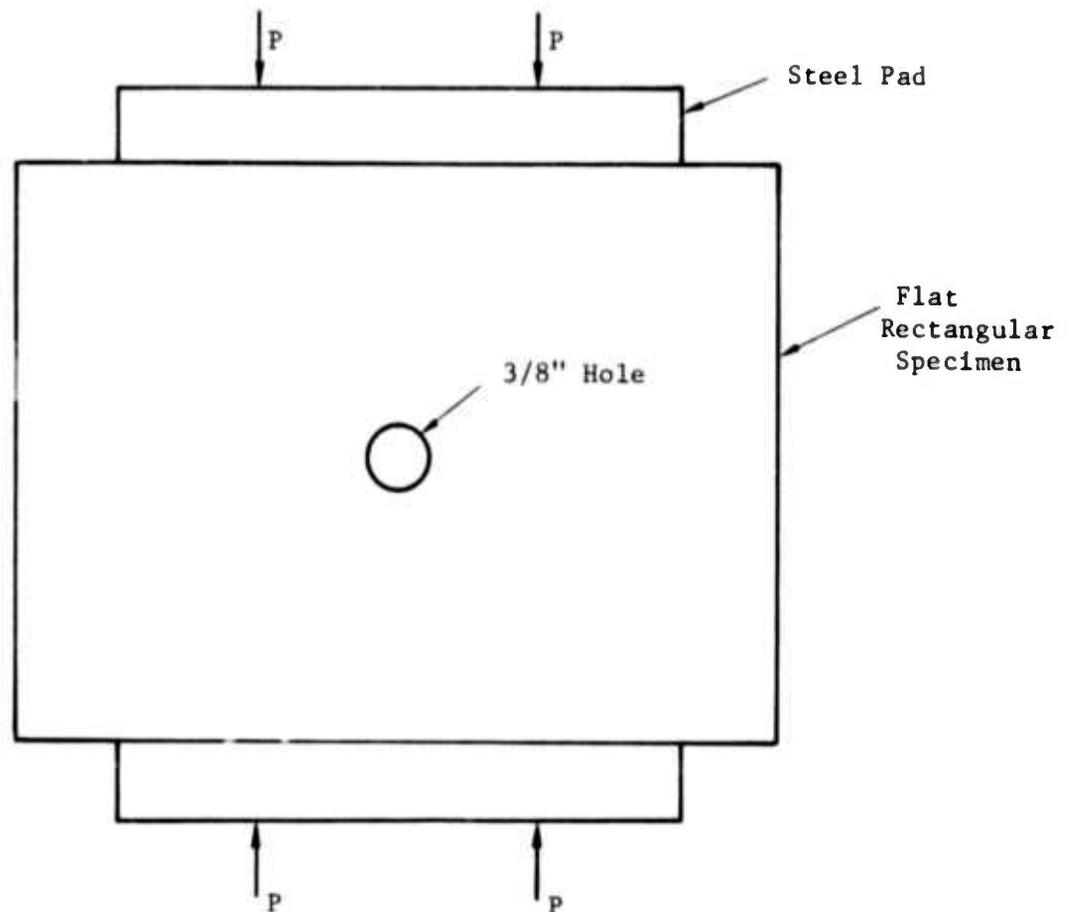The experimental set-up for the rectangular specimen is shown schematically in Figure 6.1.

Figure 6.1: Simplified schematic of flat rectangular specimen in compression. See Figure 3.9 for a photograph of the actual specimen fixture.

For this experiment, two point loads were applied to each steel pad at the top and bottom of the specimen. The stress field desired is a uniform stress σ_o in the vertical direction; however, because of bending in the steel plate, the stress field will peak under each point load, P. Additional stress peaking may occur at the ends of the steel pad where the pad stops and the specimen continues. Thus, the method of loading the specimen is expected to produce a stress field $\sigma(x,y)$ which will contain peaks and nonuniformities in addition to a primary component σ_o in the vertical direction.

For purposes of analysis, these nonuniformities will be neglected, and the stress field (before the hole is drilled) will be assumed uniform. Secondly, when the hole is drilled it will be assumed that the stress on the boundary of the specimen remains unchanged. Finally, it will be assumed that the specimen is in a state of plane stress, both before and after the hole is drilled. This latter assumption is equivalent to assuming that the drilled hole passes all the way through the (two-inch thick) flat rectangular specimen. In fact, the hole only penetrates the surface for a distance of one diameter. This fact means that the in-plane stresses will vary with the distance (call it z) perpendicular to the face of the specimen. Nevertheless, on the surface of the specimen it is thought that a plane-stress solution will be fairly accurate.

6.2 Displacements for a Plate in Plane Stress

The displacements on the surface of a rectangular plate in the plane stress subjected to a uniform stress σ_o at infinity (i.e., far away from the origin of coordinates) are given by

$$u_x = \frac{\sigma_o x}{E} = \frac{\sigma_o}{E} r \cos\theta \qquad (6.1a)$$

$$u_y = \frac{\nu \sigma_o}{E} y = - \frac{\nu \sigma_o}{E} r \sin\theta \qquad (6.1b)$$

$$u_z = - \nu \sigma_o t / 2E \qquad (6.1c)$$

where

σ_o is the applied stress (positive in tension)

E is the Young's modulus

ν is Poisson's ratio

t is the plate thickness

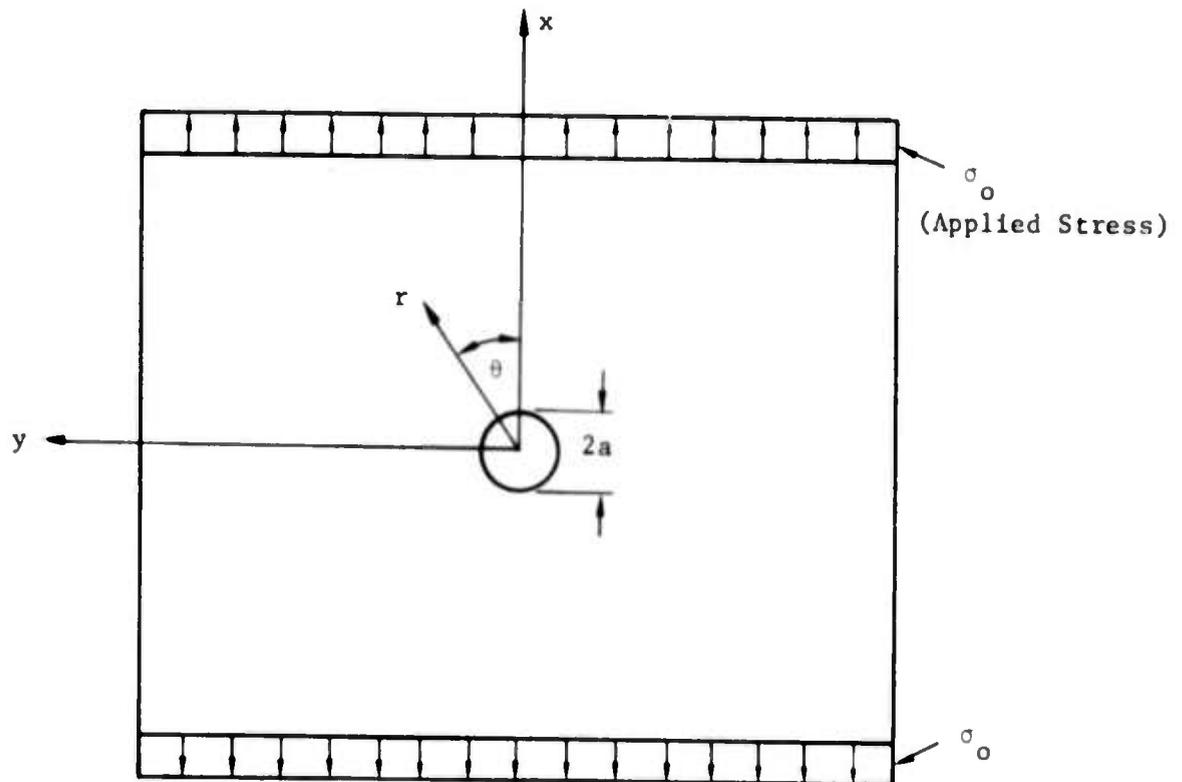u_x, u_y, u_z are the displacement in the x, y, and x directions respectively (cf. Figure 6.2).

Figure 6.2: Coordinate system for plate in plane stress.

TRW
SYSTEMS GROUP

For analysis purposes, it is more convenient to express the displacements in cylindrical coordinates. Thus, we have

$$u_r = u_x \cos\theta + u_y \sin\theta \qquad (6.2a)$$

$$u_\theta = -u_x \sin\theta + u_y \cos\theta \qquad (6.2b)$$

By substituting the expressions for u_x and u_y (Equations 6.1) into the above relations for u_r and u_θ, one finally arrives at the following non-dimensional results

$$\frac{u_r}{\sigma_o a/E} = \frac{1}{\alpha} (\cos^2\theta - \nu\sin^2\theta) \qquad (6.3a)$$

$$\frac{u_\theta}{\sigma_o a/E} = - \frac{(1 + \nu)}{2} \frac{1}{\alpha} \sin^2\theta \qquad (6.3b)$$

$$\frac{u_z}{t/2} = - \frac{\nu\sigma_o}{E} \qquad (6.3c)$$

where $\alpha = a/r$ and a is the radius of the hole (which will be discussed shortly.

When the hole is drilled in the (plate) specimen, and the stress remains σ_o at infinity, the following displacements are obtained (from Ref. 10)

$$\frac{U_r}{\sigma_o a/E} = (\frac{1 + \nu}{2}) \frac{1}{2} \left\{ (\frac{1 - \nu}{1 + \nu} + \alpha^2) + (1 + \frac{4\alpha^2}{1 + \nu} - \alpha^4) \cos^2\theta \right\} \qquad (6.4a)$$

$$\frac{U_\theta}{\sigma_o a/E} = - \frac{(1 + \nu)}{2} \frac{1}{\alpha} \left\{ 1 + \frac{2(1 - \nu)}{1 + \nu} \alpha^2 + \alpha^4 \right\} \sin^2\theta \qquad (6.4b)$$

$$\frac{U_z}{t/2} = - \frac{\nu\sigma_o}{E} \qquad (6.4c)$$

63

Th∂ doubly-exposed hologram records the difference in displacements (i.e., the incremental displacements) which occur between the two states just discussed. Thus, the interferogram responds to the displacements

$$\frac{\Delta u_r}{\sigma_o a / E} = (\frac{1 + \nu}{2}) \ \alpha \left[1 + (\frac{4}{1 + \nu} - \alpha^2) \ \cos^2\theta \right] \qquad (6.5a)$$

$$\frac{\Delta u_\theta}{\sigma_o a / E} = - \frac{\alpha}{2} \left\{ (1 - \nu) + (\frac{1 + \nu}{2})\alpha \right\} \ \sin^2\theta \qquad (6.5b)$$

$$\Delta u_z = 0$$

where

$\Delta u_r = U_r - u_r$ is the difference in radial displacements

$\Delta u_\theta = U_\theta - u_\theta$ is the difference in circumferential displacements

$u_z = U_z - u_z$, etc.

The preceding displacement increments must now be related to the fringes formed by holographic interferometry. For this purpose it is convenient to transform back to rectangular coordinates (x, y, z). Thus, using the relations

$$\Delta u_x = \Delta u_r \ \cos\theta - \Delta u_\theta \ \sin\theta \qquad (6.6a)$$

and

$$\Delta u_y = \Delta u_r \ \sin\theta + \Delta u_\theta \ \cos\theta \qquad (6.6b)$$

We have finally

$$\frac{\Delta u_x}{\sigma_o a/E} = \frac{\alpha}{2} \left\{ (5 + \nu) - (1 + \nu)\alpha^2 - (1 + \nu)(2 - \alpha - \alpha^2)\sin^2\theta \right\} \cos\theta \qquad (6.7a)$$

$$\frac{\Delta u_y}{\sigma_o a/E} = \frac{\alpha}{2} \left\{ -3 + \nu + (1 + \nu)\alpha^2 + (1 + \nu)(1 - \alpha - \alpha^2)\cos^2\theta \right\} \sin\theta \qquad (6.7b)$$

$$\frac{\Delta u_z}{t/2} = 0$$

For the incremental displacements (between exposures of the hologram in the x, y, and z directions respectively.

6.3 Generation of the Theoretical Fringe Patterns

From the theory of double-exposure holographic interferometry (Ref. 11) we know that an interference fringe is formed whenever the condition

$$\vec{\delta} \cdot (\vec{c} + \vec{s}) = \frac{(2n \pm 1)\lambda}{2} \qquad (6.8)$$

is met. In Equation (6.8)

$\vec{\delta}$ = the displacement vector

λ = wavelength of the light from the laser used to record and reconstruct the holographic images

$\vec{c}$ = unit vector in the direction from the object to the illuminating source

$\vec{s}$ = unit vector in the direction of view, from the object through the hologram to the observer

n = integer, the fringe order, ± 1, ± 2, ± 3, etc.

In general, the vectors $\vec{c}$ and $\vec{s}$ vary with the position of the point on the body (where the displacement $\vec{\delta}$ occurs). Note that the displacement of a point on the surface is also a function of position: $\vec{\delta} = \vec{\delta}(x, y, z)$. Equation (6.8) is normally used to compute the displacement field $\vec{\delta}(x, y, z)$ from an experimental fringe pattern, when the illumination and viewing vectors $\vec{c}$ and $\vec{s}$ are known.

65

For the present discussion, we have

$$\vec{\delta} = \Delta u_x \vec{i} + \Delta u_y \vec{j} + \Delta u_z \vec{k} \tag{6.9}$$

where Δu_x, Δu_y, and Δu_z are given by Equations (6.7) and $\vec{i}$, $\vec{j}$, $\vec{k}$ are unit vectors in the x, y, z directions, respectively. What will be done in this case is to compute the "theoretical" fringe pattern corresponding to the assumed stress state (i.e., the fringe pattern for drilling a hole in a uniformly stressed plate) by using Equation (6.8). The theoretical fringe pattern requires that we specify the illumination vector $\vec{c}$ and the viewing vector, $\vec{s}$, in addition to the fringe order(s) in Equation (6.8).

In the experimental set-up, the size of the holographic apparatus is such that the vectors $\vec{c}$ (illumination) and $\vec{s}$ (viewing) vary over the surface of the specimen. For the conventional problem of computing displacements from a fringe pattern, the variation of $\vec{c}$ and $\vec{s}$ are functions of position and would be included. However, for purposes of the present analysis these vectors will be assumed constant.

The values of the viewing vector $\vec{s}$ used corresponds to a view looking directly down the z-axis of the hole in the specimen. Since the viewing vector points from the object through the hologram to the observer, we have

$$\vec{s} = 0\vec{i} + 0\vec{j} + 1\vec{k} = \vec{k} \tag{6.10a}$$

(i.e., $\vec{s}$ is a unit vector along the z-axis).

The illumination vector (also assumed constant) was taken as the vector from the center of the hole in the specimen to the small diffuser in the holographic set-up. This vector was determined from the geometry of the holographic set-up as

$$\vec{c} = \frac{1}{\sqrt{3}} \vec{i} - \frac{1}{\sqrt{3}} \vec{j} + \frac{1}{\sqrt{3}} \vec{k} \tag{6.10b}$$

Finally, the results for $\vec{\delta}$, $\vec{s}$, and $\vec{c}$ of Equation (6.8) to give

$$\vec{\delta} \cdot (\vec{c} + \vec{s}) = \frac{\Delta u_x}{\sqrt{3}} - \frac{\Delta u_y}{\sqrt{3}} = \frac{(2n \pm 1)\lambda}{2} \tag{6.11}$$

66

TRW

In Equation (6.11), we have expressions for Δu_x and Δu_y as functions of r and θ from Equations (6.7). Thus, Equation (6.11) can be written in functional form as

$$f(r,\theta) - \frac{(2n \pm 1)\lambda}{2} = 0 \qquad (6.12)$$

Equation (6.12) was used to plot the "theoretical" fringes by specifying the wavelength λ a particular fringe number n, (e.g., n = 1, 2, 3, etc.) and solving for the curve in (r,θ) space for which Equation (6.12) was satisfied. In actual practice, a small FORTRAN computer program was written in which the angular position was specified (as a parameter) and then Equation (6.12) simply becomes

$$F(r;\theta,n) = F(r) = 0 \qquad (6.13)$$

a function of r only, since we are operating with a constant fringe order (n is fixed) and along a particular ray from the origin (θ is fixed). Equation (6.13) was solved for its roots r_i using Newton's method, and the root $r_i(\theta,n)$ determines a point on the nth fringe at the particular angle θ.

With the fringe order n held constant, the angle θ can then be indexed to a new value and the process repeated to give another point on the fringe curve. This procedure was readily automated and connected with a plotting subroutine to produce the "theoretical" fringe patterns.

6.4 Discussion of the Theoretical Results

The computer generated fringe pattern shown previously in Section 4.1 (Figure 4.7) is based on the experimentally measured applied stress σ_o and handbook values of granite for Young's modulus E and Poisson's ratio ν, (Ref. 12). The parameters used were as follows:

$$\sigma_o = -4200 \text{ psi (compression)}$$
$$E = 9.6 \times 10^6 \text{ psi (modulus)}$$
$$\nu = 0.18 \text{ (Poisson's ratio)}$$
$$a = 0.1875 \text{ inches (hole radius)}$$
$$\lambda = 632.8 \text{ nm (wavelength)}$$

67

The applied stress and modulus enter the equations directly as (σ_o/E) and influence the amount that the fringe loops open or close. The variation of the fringe patterns with Poisson's ratio, ν, was examined and found to be rather slight. The hole diameter, a, and the wavelength, λ, were not varied, since they are both known accurately.

The theoretical results are in qualitative agreement with the experimental fringe patterns. Both patterns have a double-lobed appearance, with the bottom lobe agreeing quite well with the theoretical pattern. However, the experimental pattern also has another lobe (which depends upon the viewing direction) off to one side, whereas the theoretical pattern is more symmetric. This discrepancy is thought to be due to one or more of the simplifying assumptions made in the analysis. For example, we know that the two-point loading (through the steel balls) in the experiment will produce a non-uniform stress distribution. Thus, the stress distribution is just approximately uniform. Furthermore, it was necessary to assume that the specimen was in a state of plane stress, and this assumption neglects the fact that the stress distribution varies with the depth of the hole. Finally, the assumption that the vectors $\vec{c}$ and $\vec{s}$ are constant is true only if the viewer and the source of illumination are "far" away from the granite specimen. In the experiment, the vectors $\vec{c}$ and $\vec{s}$ can vary by as much as 25% for a point at a radial distance $r = 1.5$ inches off the z-axis. Larger changes in $\vec{c}$ and $\vec{s}$ occur as the point in question lies at larger radial distances.

Although the effects of these simplifying assumptions could not be investigated within the temporal and financial constraints of the present contract, many of these approximations can be removed. For purposes of the present study, the simplified theoretical analysis of the rectangular specimen was felt to be adequate.

TRW
SYSTEMS GROUP

7.0 CONCLUSIONS AND RECOMMENDATIONS

A laboratory model of a holographic instrument was designed and built to operate in a simulated borehole environment. The principle of operation involves measuring strain in the side of a prestressed rock specimen due to stress relief by small side coring holes. The strains are recorded using holographic interferometry where the displacement fields are stored in fringe patterns covering the holographically recorded images of the strained surface. The holographic instrument consisted of (1) core drill module, (2) optics module, (3) laser module as well as associated electrical and plumbing connections to operate the instrument. The laboratory model incorporated many features which would be common to a field version but also included features to aid in the collection of holographic data in a laboratory. The performance of the holographic instrument in a dry and water-flooded simulated (concrete) borehole was excellent. The fringe patterns obtained from holograms made in a simulated borehole are predictable and follow a classical analysis of strain relief. The next phase will require the completion of the design of the field instrument shown schematically in Figure 7.1. This will require the following areas to be addressed.

o Capsulating a commercial laser with power supply.

o Incorporation of control circuits for remotely performing core drill operations, optics alignment, and film exposure in three directions in a borehole.

o Design of the holographic film cassette and its incorporation into the holographic optics module.

o A pressurization system to offset the down-hole head of water.

o On board water filtering equipment to provide clear view of wall surfaces.

o Integration of the three basic modules and control equipment into a support casing which has provisions for anchoring the instrument in three orientations against the sides of the borehole.

o Modification of an existing computer code which takes into account the combined geometry of the borehole and the holographic optics to provide machine inversion of observed displacement fields to principal stresses.

o Field tests of resulting instrument.

69

TRW.
SYSTEMS GROUP

   An added advantage of the optical instrument is that the holo-
graphic recording will also provide a means for inspecting the surface
of the borehole; that is, it will act as a bore "scope" since holography
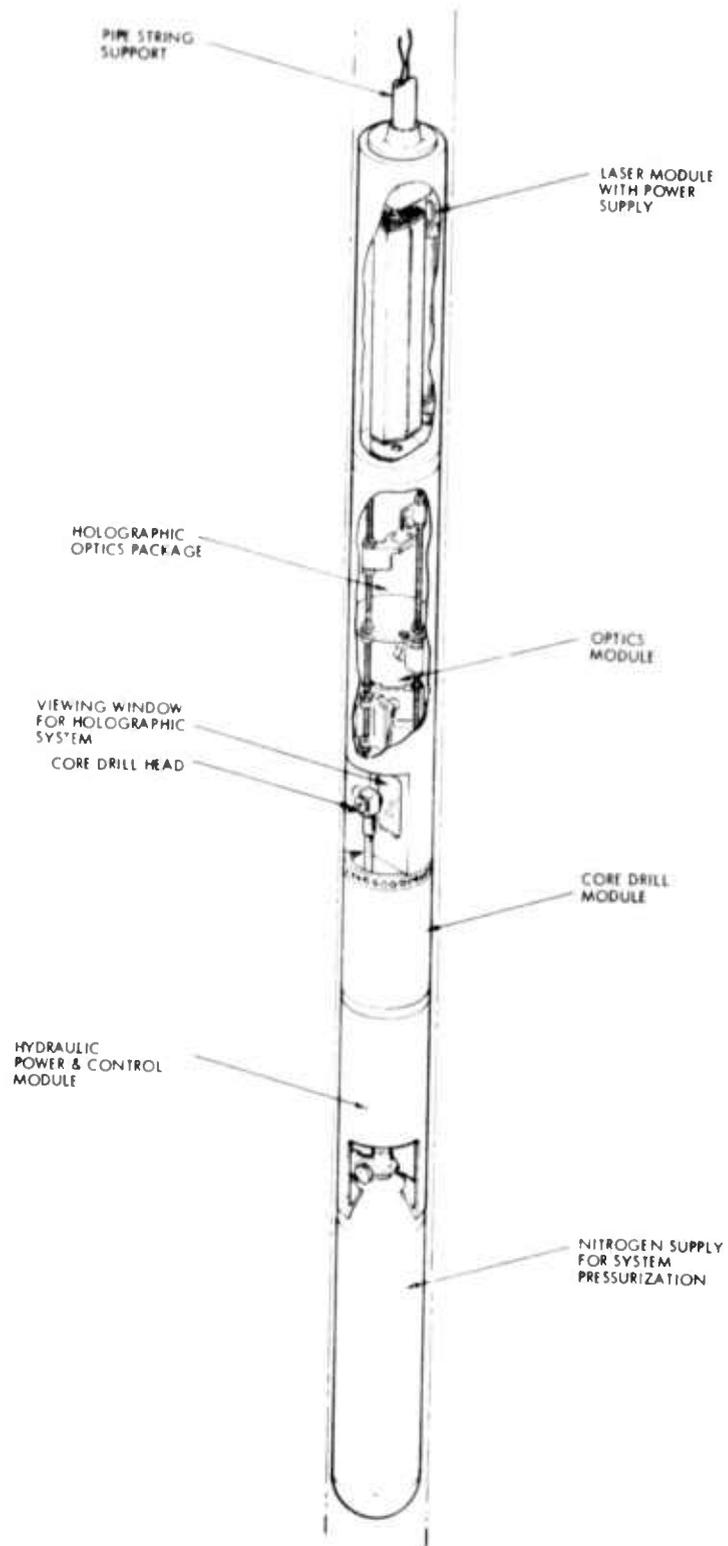will record the surface of the borehole with virtually infinite depth
of focus.

Figure 7.1: Optical in-situ stress measurement instrument.

TRW
SYSTEMS GROUP

8.0 REFERENCES

1. Brody, Brian T., "Basic Requirements for the Design of Mine Openings," Bureau of Mines Technology Transfer Seminar Proceedings, Bureau of Mines Information Circular 8585, July 25, 1972.

2. Aggson, J. R., "Bureau of Mines Borehole Deformation Gage for Determining In-Situ Stress," Bureau of Mines Information Circular 8585, July 25, 1972.

3. Pallister, G. F., N. C. Gay and N. G. W. Cook, "Measurement of the Virgin State of Stress in Rock at Depth," Proc. of the Second Congress, International Soc. of Rock Mechanics, Belgrade, 25, 1970.

4. Merrill, R. H., "In-Situ Determination of Stresses by Relief Techniques," in State of Stress in the Earth's Crust, W. R. Judd, ed., 343, Elsevier Co., 1964.

5. Aprahamian, R., J. L. Jacoby, J. D. O'Keefe, T. J. Ahrens, "Holographic Study of Wave Propagation in Granite," TRW Systems Group, DASA01-69-C-0152, 21 May 1971.

6. Aleksandrov, E. B. and A. M. Bonch-Bruevich, "Investigation of Surface Strains by the Holographic Techniques," Soviet Physics, Technical Physics, Vol. 12, No. 2, August 1967, p. 258 ff.

7. Witte, A. B., J. Fox, H. Rungaldier, "Localized Measurements of Wake Density Fluctuations Using Pulsed Laser Holographic Interferometry," AIAA Journal, Vol. 10, No. 4, April 1972, pp. 481-487.

8. Hirmatsu, Y., and Y. Oka, "Stress Around a Shaft or Level Excavated in Ground with a Three-Dimensional Stress State," Kyoto University, Faculty of Engineering Memoirs, Vol. 24, 1962, pp. 56-76.

9. Aprahamian, R., J. D. O'Keefe and K. R. Overoye, "Experimental Investigation of Fracture of Granite Under Compression," Final Report under ARPA Order No. 1579, 15 December 1971.

10. Venkatraman and Patel, Structural Mechanics with Introductions to Elasticity and Plasticity, McGraw-Hill, New York, 1970.

11. Brown, G. M., R. M. Grant and G. W. Stroke, "Theory of Holographic Interferometry," J. Acous. Soc. Amer., Vol. 45, No. 5, May 1969, pp. 116-1179.

12. Handbook of Physical Constants, Published by the Geological Society of America, Inc., S. P. Clark, Jr., Editor, 1966.

13. Evensen, D. A. to J. L. Schmidt, "Displacements in a Pre-Stressed Circular Disc with a Central Hole," TRW IOC 8522.6-73-29.

APPENDIX A - STRAIN RELIEF IN A FLAT CYLINDRICAL SPECIMEN

A numerical analysis was performed on an interference fit method of producing a radially symmetric stress distribution in a cylindrical granite disk. Calculations were used to determine the dimensions of a steel ring and the magnitude of the interference fit required to produce the desired stress levels in the cylindrical disk. The stress field would be produced by slipping a heated steel ring over the granite disk and letting it cool to create a compressive interference fit. The stress levels selected were based on the fringe densities which would result from the drilling of a stress relief corehole. The maximum fringe density criteria was 1 line/mm, since higher fringe densities would be difficult to resolve photographically.

The geometry of the stressed cylindrical disk and a typical radial displacement profile resulting from the stress relieving hole being drilled in the center of the disk is shown in Figure A.1. The displacement profile due to stress relief at the center of the specimen is a function of the diameter of the stress relieving hole and the pressure P_o on the outside perimeter of the disk. This relationship is given by Reference 13 as

$$\Delta u(r) = - \frac{(1 + 2\nu)}{1 + \nu} \frac{P_o}{E} \frac{\left(r_1^2 r_o^2\right)}{\left(r_o^2 - r_1^2\right)r} \tag{A.1}$$

where Δu = relative in-plane radial displacement when the hole is drilled

   r = variable radius

   r_1 = radius of the stress relieving hole

   r_o = outside radius of the disk

   P_o = stress on the circumference

   ν = Poisson's Ratio

   E = modulus of elasticity

As see from Eq. (A.1), the results can be scaled to any pressure since the relative displacement at any point r on the surface is
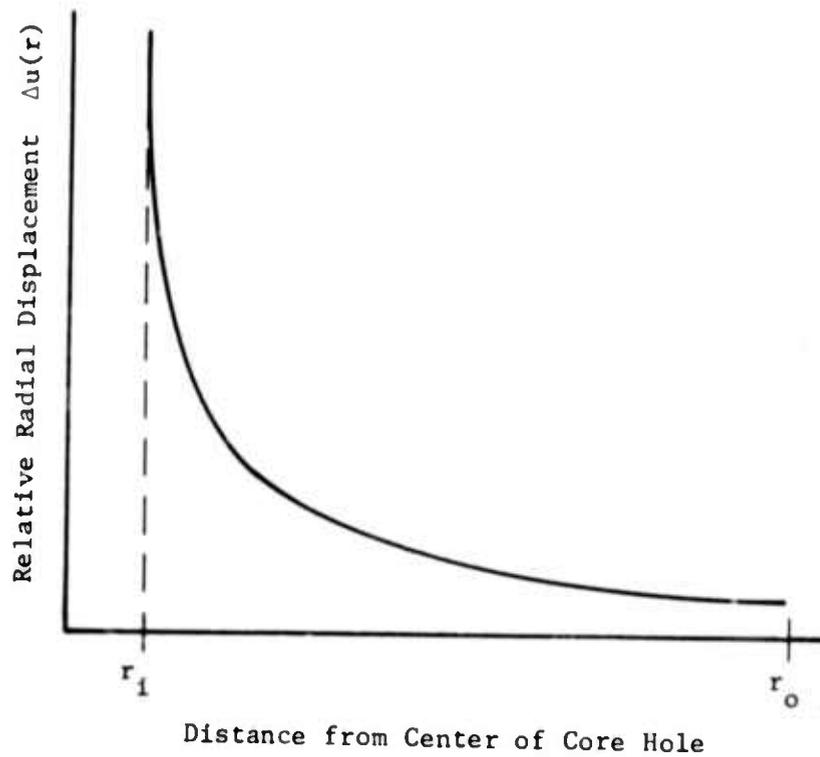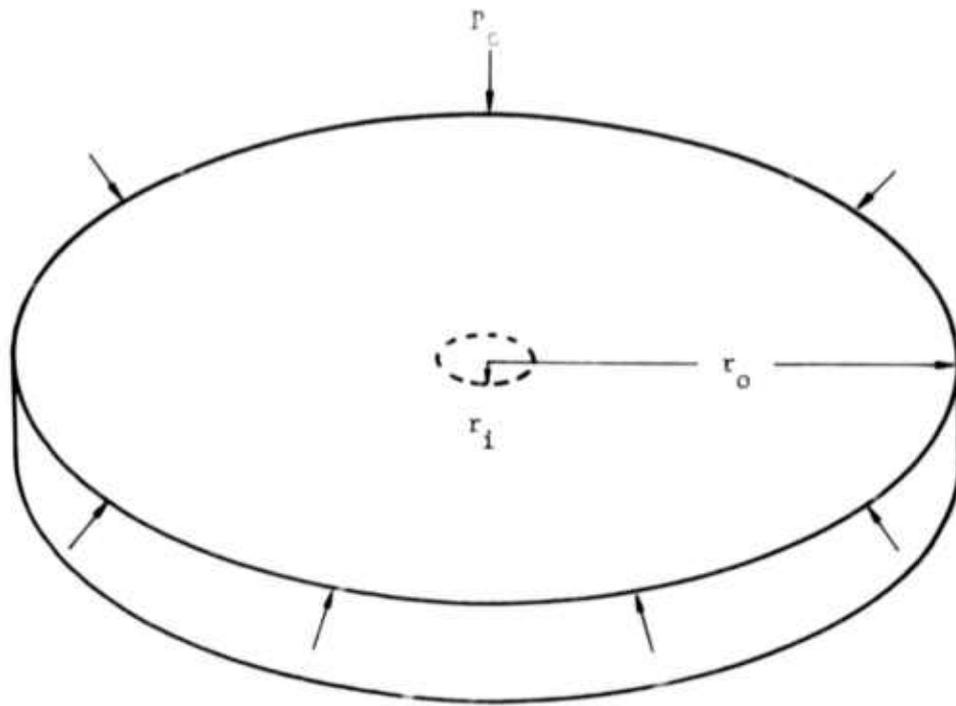
Figure A.1: The general displacement profile obtained by drilling a core hole in the center of a radially stressed cylindrical disk.

directly proportional to P_o. The outside radius of the specimen r_o is 2.80 inches while the modulus for the granite was taken as 8×10^6 psi. Using these values in Eq. (A.1), the displacement profiles $\Delta u(r)$ for two different size stress relieving coreholes are

$$\Delta u(r) = -2.35 \times 10^{-9} \frac{P_o}{r} \; ; \quad r_1 = .125 \; (1/4" \text{ diameter hole})$$

$$\Delta u(r) = -9.45 \times 10^{-9} \frac{P_o}{r} \; ; \quad r_1 = .250 \; (1/2" \text{ diameter hole}) \tag{A.2}$$

The stress field P_o combined with the holographic viewing geometry was used to plot anticipated fringe profiles produced by different size coreholes. In Figures A.2 and A.3 the fringe profile $N(r)$ is plotted for 1/4" and 1/2" coreholes at 3000 and 6000 psi stress fields. These curves should be considered accurate only in the vicinity of the corehole since simplifying assumptions were made in the equations used to derive the holographic geometry. The important factor derived from these curves is that approximately four times as many fringes would be seen for the larger corehole diameter for the same stress distributions.

Although the circular specimen is easier to analyze for stresses and deformations, practical problems prevented it from being used successfully. In particular, it was difficult to machine the steel prestressing ring to the proper tolerance on its diameter. Furthermore, the stress level is fixed (once the ring is installed) and cannot be adjusted. Accordingly, during the study the decision was made to switch over to the flat rectangular specimen discussed in Sections 3.5 and 6.0.
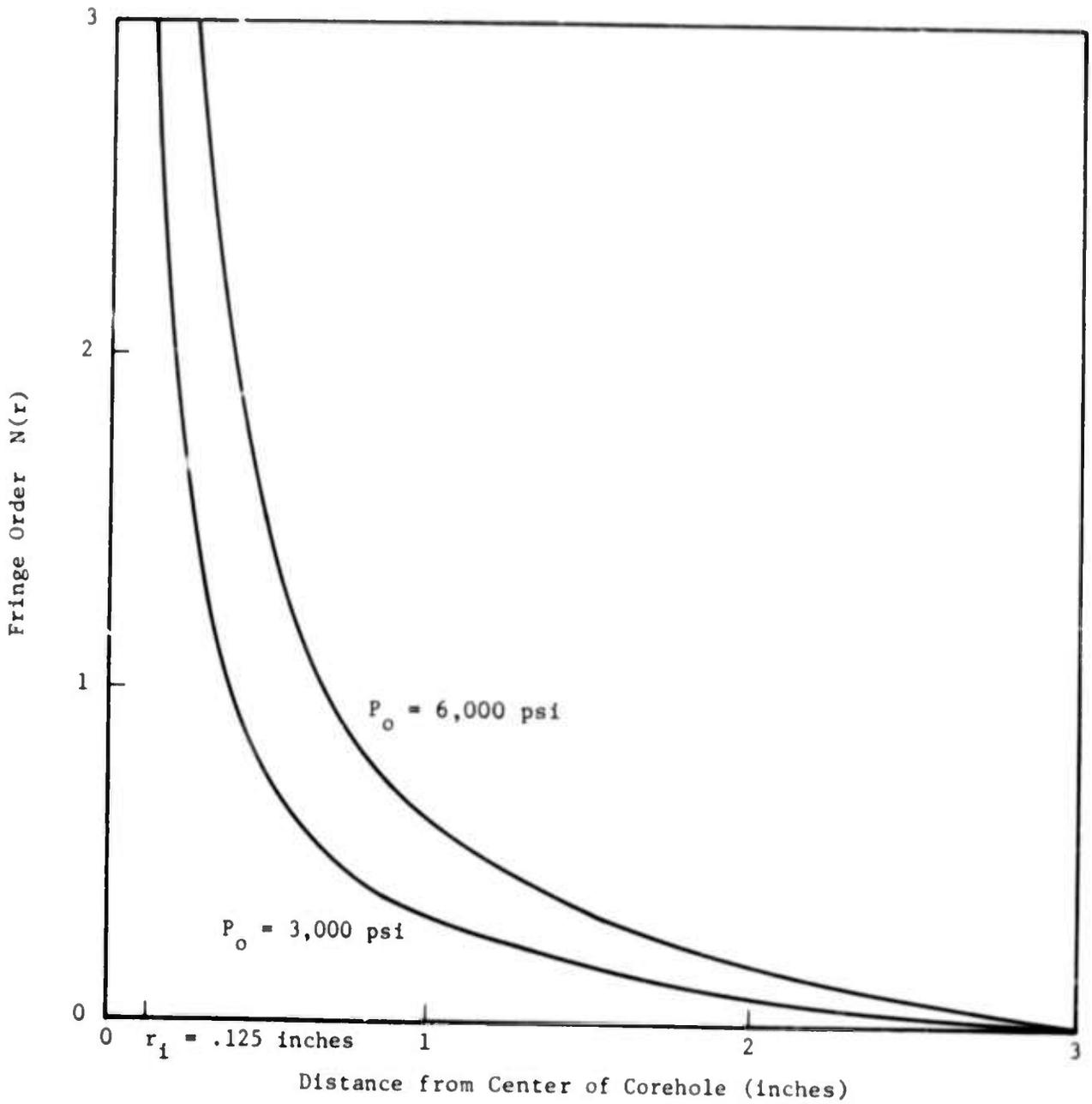
Figure A.2: Plot of calculated fringe order versus distance from center of corehole with diameter of .250 inches.
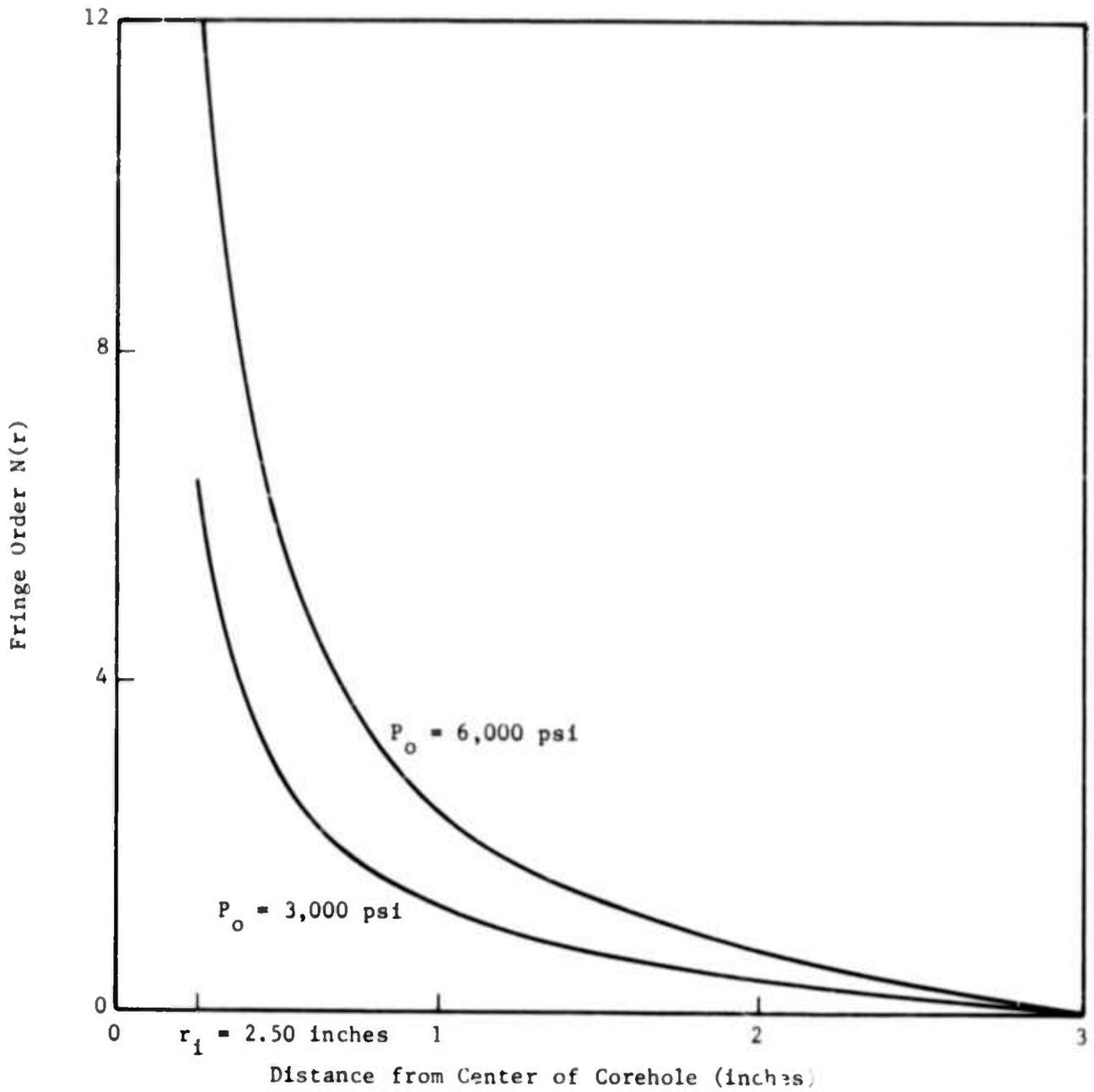
Figure A.3: Plot of calculated fringe order versus dsitance from center of corehole with diameter of .50 inches.